



1 **The role of siliceous sponges in pre-Eocene marine Si cycle from the perspective rock**

2 **mineralogy**

3 **Agata Jurkowska^{1*}, Ewa Świerczewska-Gładysz², Szymon Kowalik Filipowicz³**

4 ¹ AGH University of Krakow, Poland, Faculty of Geology, Geophysics and Environmental Protection,
5 Mickiewicza St., 30, 30-059 Krakow, Poland; jurkowska.a@gmail.com; <https://orcid.org/0000-0001-5457-9968>; Corresponding Author

6
7 ² University of Łódź, Faculty of Geographical Sciences, Department of Geology and Geomorphology,
8 Narutowicza 88, 90-139 Łódź, Poland; ewa.swierczewska@geo.uni.lodz.pl; <https://orcid.org/0000-0003-4628-2712>

9
10 ³ szymon.kowalik@10g.pl, independent researcher

11

12 **Abstract:** The process of siliceous sponge dissolution during diagenesis was interpreted not
13 only as an important part of marine Si cycle (comprising Si burial) but also as a significant
14 mechanism of chert formation (so-called “chertification”; Maliva and Siever, 1989a). Both
15 ideas were widely accepted by researches and are commonly used in geological studies. New
16 research contradicts these seminal assumptions and indicates that in pre-Eocene marine Si
17 cycle, although siliceous sponges were an important part of the ecosystems, did not play a
18 controlling role in regulating dSi (= dissolved silicon) concentration in the porewater as well as
19 in chert formation. The presented studies based on advanced mineralogical (XRD, EBSD;
20 SEM-EDS) and microtextural (SEM) analysis of rocks and sponge remnants verify the role of
21 siliceous sponges in the formation of Cretaceous siliceous rocks, by studying successions
22 deposited in similar marine environments, which contain abundant fossils of siliceous sponges
23 associated with cherts and authigenic silica polymorphs and those without them. For the first
24 time, the mineralogical and microtextural transformations of siliceous sponge loose
25 spicules/rigid skeletal networks, which led to their preservation as siliceous or pyrite/marcasite
26 infillings and also in form of limonite coatings, are presented. The data presented here about
27 the diagenesis of siliceous sponges skeletons opens the discussion on the usefulness of stable
28 isotopic studies of $\delta^{30}\text{Si}$ in geological studies of fossils of silicifiers preserved as secondary
29 silica polymorphs (opal-CT).



30

31 **Keywords:** Si cycle; cherts; opal-CT; $\delta^{30}\text{Si}$, spicule diagenesis

32

33 1. Introduction

34 The diagenetic dissolution of skeletal elements of siliceous sponges in seabed mud is an
35 important part of the biogeochemical Si cycle in marine environments comprising the Si burial
36 in sediments via the rock formation (Maliva et al., 1989; Maliva and Siever, 1989a, b; Siever,
37 1991). According to the classical model of chert formation (“chertification”), this process is
38 directly controlled by the dissolution of siliceous sponge skeletons, which are the main source
39 of dSi (=dissolved silicon) for porewater (Maliva and Siever, 1989a; b). Moreover, the
40 importance of the process of siliceous sponge spicules dissolution is highlighted by the fact that
41 it has been interpreted as a basic mechanism controlling the porewater dSi concentration
42 (Maliva and Siever, 1989a, b; Siever, 1991). Recent studies have critically verified the previous
43 model of chertification and the biotic origin of siliceous nodules, and revealed that the dSi
44 seawater concentration governing the process of silica polymorphs precipitation and chert
45 formation mainly depends on environmental abiotic factors (volcano-hydrothermal dSi sources)
46 (Jurkowska and Świerczewska-Gładysz, 2020a, b; 2024 Jurkowska, 2022). This indicates that
47 previously accepted assumptions of a significant role of siliceous sponge dissolution in a Si
48 cycle need to be better recognized in order to evaluate its importance in controlling dSi
49 porewater concentration.

50 The key point of this research is the reconstruction of the process of early diagenetic dissolution
51 of biogenic opal-A of siliceous sponge spicules within the seabed mud followed by the silica
52 polymorphs transformation leading to the formation of siliceous sponge fossils and siliceous
53 (cherts) or carbonate-siliceous (opoka) rocks and environmental factors controlling them. The
54 geological record of siliceous sponge fossil and siliceous rock enables the reconstruction of



55 mineralogical silica phase transformation as well as factors controlling them, by mineralogical
56 and microtextural studies (Jurkowska and Świerczewska-Gładysz, 2020a, b; Jurkowska, 2022).
57 This analysis cannot be replicate in laboratory conditions due to their duration of tens of
58 thousands of years (Kastner et al., 1977). The studies have been conducted in Upper Cretaceous
59 deposits of the European Basin and present different models of siliceous sponge dissolution and
60 silica polymorphs reprecipitation reflected in various types of preservation sponge skeletons in
61 a carbonate/clayey seabed mud.

62 The studies presented here have an impact not only on the recognition of rocks genesis but also
63 for evaluation of the usefulness of the rapidly developing scientific tool of $\delta^{30}\text{Si}$ measurements
64 of siliceous sponge spicules built of primary opal-A for the estimation of seawater dSi
65 concentrations (Sutton et al., 2018; Hendry, 2012). This very promising idea, which is used for
66 to determine dSi in recent and Cenozoic oceans, could potentially be transferred into Paleozoic-
67 Mesozoic fossil siliceous sponges. However, without proper recognition and documentation of
68 a diagenetic process of sponge spicules dissolution and biogenic opal-A transformations its
69 usefulness in paleontological record is doubtful. Taking into account that the process of
70 siliceous sponge skeleton dissolution is a complex series of environmentally dependent
71 polymorphic silica transformations, during which the primary signature of $\delta^{30}\text{Si}$ can be
72 changed, the detailed recognition of the mechanism of skeleton dissolution followed by silica
73 reprecipitation is essential for the use for of $\delta^{30}\text{Si}$ from skeletons of fossil sponges in the
74 geological interpretations.

75

76 **2. Seminal model (Maliva and Siever, 1989a): the role of siliceous sponge dissolution** 77 **in siliceous nodules and carbonate-siliceous rock formation**

78 The general assumptions about the role of siliceous sponges in the formation of siliceous bedded
79 and nodular cherts and flints have been summarized and presented by Maliva and Siever



80 (1989a, b), who described the model of siliceous nodule formation in Mesozoic and Cainozoic
81 deposits (Fig. 1). All the assumptions that laid the foundations for Maliva and Siever (1989a,
82 b) model of ‘chertification’ are derived by mineralogical and paleontological analysis of
83 geological record of field sections (Bromley and Ekdale, 1984; Clayton, 1984) and DSDP
84 (Deep Sea Drilling Project) cores (Heath and Moberly 1971; Von Rad and Rosch, 1974; Wise
85 and Weaver, 1974). The classical model of the formation of siliceous cherts and flints, which
86 has been generally accepted in the literature and extended for other carbonate siliceous rocks
87 (e.g. opoka, gaize, Sujkowski, 1931; Pożaryska, 1952), describes this authigenic process as a
88 complex series of dissolution/precipitation reactions triggered by changes of geochemistry within
89 the seabed mud and followed by later diagenetic silica polymorphs maturation, which finally
90 led to formation of siliceous rocks. The presented model involves four main stages of silica
91 polymorphs precipitation (Fig. 1) in combination with the assumption that essential for the silica
92 polymorphs precipitation elevated dSi seawater concentration (at least of a level 10–60 ppm;
93 250–1000 μM ; (Siever, 1991)) was achieved due to siliceous sponge (opal-A) dissolution.
94 The general argument presented in the literature confirming that the siliceous sponge spicules
95 have been the main source of dSi for siliceous rock formation is based on the observation of a
96 presence fossils of sponge spicules and/or voids left after their dissolution within the siliceous
97 nodules/carbonate siliceous rocks. In many studies, although the sponge fossils are very rare,
98 they were treated as an argument confirming the assumption of biogenic dSi origin. The
99 assumption of biogenic dSi origin was so grounded even with the absence of siliceous sponge
100 remains in the rocks, it has been explained by its complete dissolution (Maliva and Siever,
101 1989a, b). The other arguments that have been used to confirm biogenic origin of dSi for
102 siliceous rock formations was based on a correlation between facies chert distribution and
103 siliceous fauna migration in Earth history (Maliva et al., 1989). This idea has been critically
104 discussed in our previous article (Jurkowska and Świerczewska-Gładysz, 2024) and in light of



105 new data summarized there, this argument can no longer be used to confirm the biogenic origin
106 of siliceous nodules. The additional statement assumed in seminal work of Maliva and Siever
107 (1989a, b) concludes that besides the siliceous skeletons, there is no probable source of dSi in
108 seawater. This last argument was also critically discussed (Jurkowska and Świerczewska-
109 Gładysz, 2024 and literature cited therein) and, based on new data, the dSi source of
110 volcanic/hydrothermal origin connected with LIP (Large Igneous Provinces) activity was
111 pointed out. To sum up from the main three arguments which has been used to confirm the
112 biogenic origin of cherts in the classical model (Maliva and Siever, 1989a, b) the mechanism
113 of siliceous sponge spicules dissolution has not been tested by using new analytical techniques
114 as a potentially controlling factor of dSi concentration in porewater.

115

116 **3. Siliceous sponge – sediment system an methodological approach**

117 The role of siliceous sponges in the chertification process involves the siliceous skeleton
118 dissolution making them a source of dSi to the seawater, which directly controls the overall dSi
119 concentration and is followed by abiotic silica polymorphs precipitation (Jurkowska, 2022).
120 The process of biogenic opal-A dissolution and silica precipitation is geochemically dependent
121 and involves chemical interaction between the external environment and distinctive
122 microenvironment that forms around and inside of the decaying sponge. The geochemical
123 environmental factors which control the silica dissolution and its reprecipitation could be
124 characterized as dSi concentration of seawater/porewater, organic matter (OM)
125 content/distribution and mineralogical composition of the seabed mud (content of carbonates
126 and clays) (Williams and Crerar, 1985; Kastner et al., 1977). Sponge morphology (presence of
127 loose or fused spicules, wall thickness) and organic matter content control the ability to the
128 chemical interaction between the external environment and microenvironment of decaying
129 sponge remnants, involving the possibility of the dSi migration from the siliceous skeleton



130 dissolution to the seawater/porewater (Jurkowska and Świerczewska-Gładysz, 2020a; b;
131 Jurkowska, 2022). Assuming the process of siliceous sponges skeleton dissolution is dependent
132 on geochemical conditions of the surrounding environment and interaction of a porewater with
133 decaying sponge body to recognize the complex mechanism of the sponge siliceous skeleton
134 dissolution and silica reprecipitation, and environmental and internal (sponge morphology)
135 factors controlling these processes, we designed the mineralogical/microtextural studies of
136 various sponge fossils.

137 The methodological background for testing the role of siliceous sponge dissolution in the
138 formation of siliceous rocks is based on a selection of siliceous rocks (cherts) and carbonate-
139 siliceous (opoka) sedimentary rocks deposited during a time interval in which the siliceous
140 sponges have been indicated as a source of dSi for their formation (Calvert, 1974, 1977; Maliva
141 and Siever, 1989a; b; Siever, 1991). For comparative analysis, we choose rocks (limestones and
142 marls) in which the fossils of siliceous sponges are common, but the silica polymorphs have
143 not been detected in previous geological studies. We chose the successions deposited under
144 similar marine conditions (carbonate environment) during a relatively short stratigraphic range
145 (Upper Cretaceous: upper Turonian-lower Coniacian, lower-middle Campanian and upper
146 Campanian-lower Maastrichtian) and in the small geographic area of one depositional
147 epicontinental basin (southern part of the Polish Basin).

148 The primary environmental factor that affects the potential for siliceous sponge skeleton
149 dissolution and silica precipitation is seawater dSi concentration (Kastner et al., 1977; Williams
150 and Crerar, 1985). Generally, during the Earth history, seawater dSi concentration was below
151 the threshold opal-A precipitation ($<1200 \mu\text{M}$) (Siever, 1991; see also Jurkowska and
152 Świerczewska-Gładysz, 2024) which means that seawater chemistry promoted siliceous sponge
153 dissolution, indicating that siliceous skeletons potentially could be a good source of dSi in
154 seawater/porewater for siliceous rock formation. To test the impact of different dSi



155 concentration on the rate of siliceous sponges dissolution and its reprecipitation, we chose the
156 Campanian-Maastrichtian sections of opoka intercalated with cherts and marls, for which
157 different dSi concentration during deposition have been indicated (Jurkowska and
158 Świerczewska-Gładysz, 2020a; b). We extended the analysis to the upper Campanian-lower
159 Maastrichtian sections in which the opoka was deposited in a similar environment and have
160 asimilar mineralogical composition to the aforementioned opoka samples (see opoka
161 mineralogical classification in Jurkowska, 2022; Jurkowska and Świerczewska-Gładysz, 2022),
162 but is not interlayered with cherts and contains significantly more abundant voids left after
163 spicule dissolution, dispersed in a rock matrix and body-preserved sponges, whose skeletons
164 are also usually dissolved and pieces of siliceous network are rarely preserved (Jurkowska and
165 Świerczewska-Gładysz, 2020b).

166 Another factor that affects the siliceous sponge decomposition and dissolution of its skeleton
167 in sediment, as well as the silica polymorphs precipitation during diagenesis, is the presence
168 and distribution of organic matter (OM) within the seabed mud. The process of OM
169 aerobic/anaerobic microbial decomposition in the sediment column (so-called redox-cascade)
170 controls the geochemistry of the environment and triggers the diagenetic changes through
171 fluctuations in the pH and Eh conditions of porewater circulating within the seabed mud. This
172 is crucial for silica polymorph precipitation, for which the available alkalinity and Mg^{2+} ions
173 are essential and can only be achieved through microbial activity within the seabed mud
174 (Zjistra, 1987, 1994; Jurkowska, 2022; Meister et al., 2022). Under extremely oligotrophic
175 conditions, where the amount of OM in the seabed mud is decreased, the rate of microbial
176 decomposition of OM does not trigger the geochemical changes essential for alkalinity
177 production necessary for silica polymorphs precipitation. If the decomposition of OM starts
178 within interspicular spaces (which are cut off from the external environment), it can create a
179 microenvironment inside these spaces that is geochemically different (e.g. anaerobic



180 conditions) from surrounding seabed mud (Jurkowska and Świerczewska-Gładysz, 2020a). In
181 this study, the recognition of the influence of OM presence and distribution on dissolution of
182 siliceous sponges will be tested by studying specimens from the upper Turonian limestone for
183 which oligotrophic conditions were indicated (Jurkowska et al., 2018; Płachno et al., 2018), and
184 upper Turonian-lower Coniacian marls, in which the close microenvironment of decaying
185 sponge remnant will be analysed.

186 The last significant environmental factor which strongly affects siliceous sponge dissolution
187 and controls the silica polymorph precipitation is the primary (non-authigenic) mineralogical
188 composition of the sea bottom mud (Isson and Planavsky, 2018). In the studied sections, which
189 represent a relatively monotonous mineralogical composition (Jurkowska, 2022), this
190 parameter is expressed in the variable content of detrital clays. Clays affect significantly the
191 rate of silica polymorph dissolution and nucleation during diagenesis by retarding of the whole
192 process and by scavenging dSi and free space available for precipitation from newly formed
193 silica phases (Kastner et al., 1977; Isson and Planavsky, 2018; Jurkowska, 2022).

194 Non-environmental factors which also have a significant impact on the dissolution of silica
195 spicules and their preservation are features of sponges such as the structure of the skeleton of
196 individual sponges and the amount of soft body, which influences the quantity of organic matter
197 delivered by the dead sponge to the sediment. The rigid skeletal network of some sponges
198 favoured its preservation as bodily preserved fossils and created the a close microenvironment
199 around the decaying organic remnants. This rigid skeleton consists of articulated spicules called
200 desmas, which are found in some demosponges (belonging to the informal lithistida group), or
201 is formed by fused spicules (hexactins or lychniscs), occurring in two groups of hexactinellids
202 (Hexactinosida and Lychnicosida). In other groups of hexactinellids and demosponges, the
203 skeleton consists of loose spicules that disperse after the breakdown of the soft body. The
204 amount of soft body is mainly related to the thickness of the sponge wall. Most of the



205 demosponges noted in the studied section are represented by conical, cylindrical or bulbous
206 bodies with thick wall. In contrast, hexactinellids are dominated by vase-, plate- or tube-like
207 specimens with very thin walls (their thickness is usually 2–3 mm, and only occasionally
208 reaches 5 mm).

209

210 **4. Materials and methods**

211 All studied sections were deposited in Late Cretaceous European Basin under the carbonate
212 pelagic conditions of low terrigenous influx (opoka, cherts) and under the input of detrital
213 clays (limestone, marls). The oldest studied rocks are upper Turonian limestones (of the Marly
214 Limestone Unit) and upper Turonian-lower Coniacian marls (of the Upper Marls Unit) forming
215 ca. 35 m section of Opole area (e.g. Alexandrowicz and Radwan, 1973; Walaszczyk, 1988;
216 Kędzierski and Uchman, 2015; Świerczewska-Gładysz et al., 2019) (Tab. 1). These deposits
217 are exposed in the Folwark quarry, where paleontological and taphonomic studies of siliceous
218 sponge remains were conducted in two lithologies: marls and limestones. To confirm the
219 macroscopic observation of lithological type the quantitative and qualitative XRD analyses of
220 rocks mineralogical composition has been performed. The results indicate that the limestones
221 are mostly composed of calcium carbonate (94%), clays (illite-smectite) (5%), and an
222 insignificant amount of detrital quartz (1%). The marls can be distinguished from limestone by
223 lower calcium carbonate content (84%), higher clays (illite-smectite) (11%), and detrital quartz
224 content (5%). The studied upper Turonian-lower Coniacian carbonate rocks do not contain
225 silica polymorphs as a rock component, although siliceous sponge remnants are common.
226 Sponge assemblages from this section are dominated by body preserved hexactinellid sponges
227 with rigid skeleton, the body preserved lithistids are extremely rare, while rare siliceous sponges
228 without rigid skeleton are noted mainly in marls as a loose spicules or their moulds



229 (Świerczewska-Gładysz, 2012a; Świerczewska-Gładysz and Jurkowska 2013; Świerczewska-
230 Gładysz et al., 2019).

231 The other types of rocks that have been analysed are lower-middle Campanian (the rock which
232 contain opal-CT forming a siliceous framework structure (Jurkowska and Świerczewska-
233 Gładysz, 2022) of Miechów Synclinorium (MS) and middle Campanian-lower Maastrichtian
234 opoka middle Vistula River valley (MVR), lower-middle Campanian cherts (the siliceous
235 nodules primary composed of opal-CT) and marls of MS. The mineralogical composition of
236 these rocks of both regions has been studied in a previous works (Jurkowska and Świerczewska-
237 Gładysz, 2020a, b) and summarized in Jurkowska (2022; Tab. 1). Observation and sampling
238 was carried out in several outcrops: Dziurków, Piotrawin, Raj N., Pawłowice Cm, Dorotka
239 (MVR), Wierzbica, Pniaki, Jeżówka 2, Rzeżuśnia, Biała Wielka (MS) (Tab. 1). All studied
240 rocks contain a variable amount of authigenic opal-CT, which indicates the early diagenetic
241 precipitation of silica polymorphs and remnants of siliceous sponges. Spicules of non-lithistid
242 demosponges or voids after them are very numerous in opoka (Świerczewska-Gładysz 2012b;
243 Jurkowska and Świerczewska-Gładysz, 2020a, b), but are also present in marls and cherts
244 (Jurkowska and Świerczewska-Gładysz, 2020b). The macrofossils of sponges in studied
245 sections are represented by body-preserved specimens of hexactinellids and demosponges with
246 rigid skeletal network (e.g. Bieda, 1933; Hurcewicz, 1966, 1969; Świerczewska-Gładysz, 2006,
247 2016), and rare remains after large loose spicules of hexactinellids without rigid skeletal
248 network (Świerczewska-Gładysz and Jurkowska, 2013). The fossils have been collected from
249 the entire succession in each section, while microscopic analysis of sponge remains has been
250 performed on samples collected from each section at intervals of 1m from lithologically
251 monotonous sections and from different rock types if the lithological difference has been
252 observed (Tab. 1).



253 The second line of studies comprised microtextural studies, which were based on detailed SEM
254 observations (using an FEI QUANTA 200 scanning electron microscope) in three modes: SE
255 (secondary electrons), backscattered electrons (BSE) and a mix (combination of both previous
256 modes) to analyse the state of preservation and microtexture of siliceous sponges remnants
257 (loose spicules or spicules forming rigid skeletal network). The SEM observations have also
258 been performed on rock surrounding the sponge remnants and rock chips representing the
259 lithology from which the fossils originate. From the last ones also the insoluble residuum of 0.5
260 cm and 0.63 fraction has been analysed. The insoluble residuum has been prepared according
261 to the protocol describe in Jurkowska et al. (2019).

262 The second line of studies comprised the mineralogical recognition of sponge remnants, which
263 was realized through SEM-EDS, XRD, and EBSD analyses. For those samples from which
264 there was a possibility to gain enough material to perform XRD studies, those analyses have
265 been performed. The SEM-EDS analysis combined with XRD data has been used to recognize
266 the distribution and microtextural features of minerals representing polymorph groups. The
267 EBSD studies have been performed to trace the distribution of iron sulfides (pyrite and
268 marcasite) and barite within the sample. For these analyses, the polished sample surface was
269 examined in a scanning electron microscope FEI Versa 3D (FEI Company, Hillsboro, Oregon,
270 USA). The SEM observations were conducted using an electron backscatter diffraction (EBSD,
271 Symmetry S-2, Oxford Instruments Nanoanalysis, High Wycombe, UK) detector. To prevent
272 sample charging, the microscope was operated at 20 kV and ~12 nA in low vacuum mode at 20
273 Pa. The EBSD detector was operated in "Speed 2" mode, with a 156x128 pixel resolution and
274 around 300 patterns per second. Aztec (ver. 6.1, Oxford Instruments Nanoanalysis) software
275 was used to index the diffraction patterns. Hough transform resolution was set to 70, and 12
276 detected bands were used for indexing. The presented maps are "raw data" and were not
277 subjected to any cleaning or modification.



278 **5. Results and comments**

279 *5.1 The state of preservation and mineralogy of sponge skeletons*

280 In all studied lithologies, the loose spicules and skeletal network that are preserved as siliceous
281 remains are composed in different ratios of opal-CT (6–82%) and nano- α -quartz. The quartz
282 that builds the sponges' skeletal components show a smooth and uniform microtexture (Fig.
283 2a). On the surface of siliceous spicules (loose or forming a rigid skeletal network) different
284 types of dissolution remarks are visible, as cavernous pattern, rounded and platy dissolution
285 remarks (Fig. 2b). Usually, the external nano- α -quartz surface is overgrown by a single, dense
286 layer of opal-CT with well-visible blades (Fig. 2c) and/or early forms of embryonic opal-CT/"
287 Mg-rich clays" (Jurkowska and Świerczewska-Gładysz, 2020a) or a mixed opal-CT clayey
288 layer (Fig. 2d). The rounded dissolution features are secondaryily infilled by single lepispheres
289 of opal-CT of variable sizes (10–60 μm) and shapes (rounded to mushroom-like shapes) (Fig.
290 2e). Those opal-CT lepispheres show smooth microtexture without visible crystallized blades
291 and probably represent early forms of opal-CT, while their shape is controlled by the free space
292 available for precipitation. The space inside the spicules could be infilled by smooth lepispheres
293 of opal-CT (Fig. 2a) and porous or smooth silica, probably of quartz composition (Fig. 2f), or
294 homogeneous dense mass of mixed opal-CT and nano- α -quartz (Fig. 2g). Rarely, the only
295 preserved remnants are the spicule infillings composed of smooth opal-CT lepispheres
296 cemented by porous silica, while the external layer of nano- α -quartz is not preserved (Fig. 2h).
297 Another mineral that infills the voids left after the dissolution of siliceous sponge skeletal
298 elements is pyrite with subordinate marcasite. The microtexture of pyrite and marcasite
299 infillings is smooth on the outer part, while on the inside, the pyrite crystals are visible and the
300 void left after the dissolution of the area around the central canal is still preserved (Fig. 3a, b).
301 In some specimens, the external surface of the skeleton (consisting of loose ectosomal spicules
302 and/or the external part of rigid choanosomal network) represents two different mineralogies of



303 pyrite with marcasite with preserved remnants of siliceous (mixed opal-CT/nano- α -quartz)
304 spicules (Fig. 3c). In a few specimens, the voids left after the dissolution of the area around the
305 central canal are infilled by barite (Fig. 3b).

306 Euhedral pyrite crystals outline the voids left after the dissolution of loose spicules and the
307 skeletal network of siliceous sponges (Fig. 3d). The pyrite crystals are of cubic, pyritohedral to
308 octahedral crystal morphology, usually of uniform sizes (1–10 μ m). Rarely, pyrite framboids
309 are visible, of uniform sizes (3–6 μ m), usually associated with very small (<1 μ m) pyrite
310 crystals. In most samples, pyrite crystals show oxidation remarks (Fig. 3e) and corrosion pits
311 (compare: Chen et al., 2022) and are associated with visible lumps of organic matter (Fig. 3e).

312 Another type of mineralogy observed in studied paleontological material is ferrigenous
313 (representing various type of minerals of the limonite group: lepidocrocite, goethite, and
314 hematite) and mixed pyrite and ferrigenous coatings outlining the previously siliceous skeleton,
315 which is mostly dissolved (Fig. 3f). Preserved fragments of a siliceous skeleton built of mixed
316 opal-CT/nano- α -quartz structure are rare. A variety of different microtexture of ferrigenous
317 coatings is observed among this state of preservation and could be described as homogenous
318 mass forming a smooth texture inside and with a cavernous pattern on the outside of the sponge
319 spicule (Fig 3g), fibrous and fuzzy microtexture, and blocky microtexture (Fig. 3h). The pyrite
320 with limonite coatings is represented by euhedral pyrite crystals (sometimes forming
321 framboids) of uniform sizes, which are covered by layers of limonite minerals.

322 The remnants of the presence of siliceous sponges are also recorded as voids left after spicules
323 dissolution, preserved due to the existence of an external single-layer coating of silica, which
324 microtexturally resembles opal-CT. The voids left after spicules have the original shapes and
325 sizes of the spicules (Fig. 3i, j). Whether this layer is an external zone formed due to infilling
326 by secondary silica polymorphs of the original spicule or formed as a sediment layer
327 surrounding the original spicules is not known. This type of preservation is very common and



328 mostly represents megascleres of non-lithistid demosponges (Fig. 3i), but is also observed in
329 remains of other siliceous sponges (Fig. 3j) (Jurkowska and Świerczewska-Gładysz, 2020a, b).

330

331 *5.2 First factor: impact of dSi concentration on the rate of dissolution of sponge skeletons and*
332 *precipitation of silica polymorphs*

333 In Campanian cherts and chert nodules with flint cores (for the macroscopic description and
334 mineralogy details, see: Jurkowska and Świerczewska-Gładysz, 2020b) among the spicules,
335 oxeas and triaenes of non-lithistid demosponges dominate (Fig. 3k) while the loose hexactines
336 and root tufts of lyssacinoids, fragments of the rigid skeletal networks of lithistids (Fig. 3l),
337 and hexactinellid sponges (lychniscosidan and hexactinosidan) are less common (Jurkowska
338 and Świerczewska-Gładysz, 2020b). Most of the loose spicules and the fragments of the skeletal
339 network are siliceous (Fig. 3k, l) and are built of a single outer layer of homogeneous mass of
340 nano- α -quartz (sometimes covered by single fibrous layer of opal-CT (Fig. 2c) and internal
341 lepispheric opal-CT infillings (Fig. 2e, f), which are mineralogically and microtexturally
342 different from the surrounding cherts built of large lepispheres (20–30 μ m) of opal-CT or
343 siliceous rock network (Jurkowska and Świerczewska-Gładysz, 2020). The combination of
344 observations that the boundaries of chert nodules do not overlap the outlines of sponge
345 macrofossils and that silica polymorphs of chert nodule present different microtexture than
346 silica infilling the voids left after spicules, indicate that the process of chert nodule formation
347 was generally independent from the siliceous sponge skeleton dissolution and/or affected by it
348 to a small extent (Jurkowska and Świerczewska-Gładysz, 2020). Although the chemical
349 interaction and dSi migration between the dissolving sponge skeleton and surrounding mud
350 environment must exist, the dSi diffusion between the seawater and porewater was the main
351 process which controlled the dynamic balance of dSi concentration, which governs the opal-A
352 dissolution, silica precipitation inside the void left after skeleton dissolution and and the



353 formation of cherts. The infilling of the siliceous remnants of the sponge skeleton by secondary
354 authigenic silica polymorphs indicates that dSi migrates back into the voids left after skeleton
355 dissolution, probably after the chert precipitation or the chemical balance between the
356 dissolving siliceous skeleton and surrounding environment of chert was established at a dSi
357 level enabling for the authigenic silica precipitation inside the voids. Moreover, the existence
358 of dissolution remarks on a siliceous infillings of siliceous sponges indicates that after the
359 precipitation of siliceous infillings of voids left after spicules (Fig. 2b), the dSi level in
360 surrounding environment declined, triggering the further authigenic silica dissolution. The
361 dynamic interaction governing silica dissolution and precipitation was realized in the studied
362 system via dSi diffusion between three sites: seawater, cherts (by porewater) and opal-A sponge
363 skeleton, in which the first and the last acted as dSi source, while cherts and voids left after
364 spicule dissolution were dSi sinks. The process behind the dSi migration from the source to the
365 site of precipitation is Landmesser diffusion (Jurkowska and Świerczewska-Gładysz, 2020b,
366 2024) and indicates that although the siliceous sponge skeletons, through their dissolution, acted
367 as a source of dSi for the formation of siliceous nodules, seawater was the main source of dSi,
368 providing the constant dSi concentration at the level of opal-CT during the chert formation, as
369 well as precipitation of siliceous infillings of voids left after spicules (Jurkowska and
370 Świerczewska-Gładysz, 2020b). If the sponge skeletons were the main dSi source, such an
371 inflow would not be possible, and overall dSi concentration would be lower due to dSi diffusion
372 through the seawater, moreover, the siliceous infillings of voids left after spicules would not be
373 formed because after the spicule dissolution the whole process would stop.

374 The SEM observations conducted in this research also enable the reconstruction of the process
375 of the spicule dissolution followed by silica polymorphs precipitation inside the voids left after
376 spicules dissolution (Fig. 4). The process of dissolution started when the opal-A began to absorb
377 foreign ions and transformed into an intermediate form of opal-A' without any microtextural



378 changes. The dissolution started from a central canal within spicules and then their surface (see
379 e.g. Rützler and Macintyre, 1978; Bertollino et al. 2013, 2017; Costa et al. 2021), which led to
380 the complete dissolution of opal-A'. The voids left after spicule dissolution were imprinted in
381 rock by precipitating within the sediment opal-CT lepispheres (Fig. 4). In the studied
382 environment, all the essential factors necessary for silica polymorphs precipitation were
383 available. The dSi concentration, which is the primary factor necessary for silica polymorphs
384 precipitation, was available due to high seawater dSi concentration, while the other Mg^{2+} ions
385 and alkalinity were also present due to calcite and aragonite dissolution triggered by the pH
386 drop during the microbial decomposition of OM (Jurkowska and Świerczewska-Gładysz,
387 2020a; 2022). Inside the voids, the first phase to precipitate was an opal-CT, forming rounded
388 lepispheres of variable sizes and each of them acted as site and source for the diffusing dSi.
389 Between the lepispheres, when the dSi concentration dropped to the level of quartz precipitation
390 ($10 \text{ ppm} = 250 \text{ } \mu\text{M}$), the quartz started to precipitate, but its growth was prevented due to
391 simultaneously occurring dissolution initiated by dSi diffusion controlled by precipitating opal-
392 CT lepispheres (Fig. 4). When the dSi declined, the external layer of poorly formed quartz
393 crystallized, followed by the precipitation of a thin layer of early fibrous opal-CT forms or early
394 embryonic forms of opal-CT/"Mg-rich clays" under elevated dSi concentration or dissolution
395 (visible dissolution remarks) when dSi concentration declined.

396

397 *5.3 Second factor: the impact of organic matter content (OM) on dissolution of skeleton*
398 *remnants of siliceous sponges and silica polymorphs precipitation*

399 *5.3.1 The OM content and distribution in the sediment*

400 In the studied succession of Folwark quarry, the limestone of the Marly Limestone Unit was
401 deposited under oligotrophic conditions dominated by opportunistic organisms (calcispheres-
402 pithonellid assemblages – D. Rehakova pers. comm (Fig. 5a) (Jurkowska et al., 2018; Dias-



403 Brito, 2000) or those using the distinctive feeding strategy (*Lepidenteron mantelli* – Jurkowska
404 et al., 2018) to survive in an environment impoverished with biogenic elements. The
405 oligotrophic conditions are also well tolerated by hexactinellid sponges, which are the most
406 numerous group of fossils in these layers (Świerczewska-Gładysz, 2012a; Świerczewska-
407 Gładysz et al., 2019). Our observations indicate that in such an environment, diagenetic changes
408 (dissolution followed by authigenesis of newly formed minerals) were limited because the
409 overall decreased OM content did not trigger effective fluctuations of the environmental
410 geochemistry during the microbial OM decomposition. In the rock matrix, the only observed
411 authigenic mineral phases are rare newly-formed small (10–15 μm) calcite grains of rounded
412 to subhedral shapes, which are incorporated into the coccoliths carbonate rock matrix (Fig. 5b).
413 The allomicritic grains of calcite did not show any signs of dissolution, indicating that only a
414 slight drop in pH to a level where the aragonite elements and small calcite grains undergo
415 dissolution took place during early diagenesis. The absence of silica polymorphs in the rock
416 matrix or infillings of voids after spicules dissolution could be caused by diminished rate of
417 OM in the sediment due to oligotrophic conditions, which have a limiting effect on silica
418 polymorphs precipitation. The sponge skeleton are preserved as mixed euhedral pyrite with
419 subordinate ferrigenous (limonite group) coatings outlining the previous siliceous skeleton (Fig.
420 5c, d, e). This indicate that although the siliceous sponge skeleton undergoes dissolution and
421 deliver the dSi to seawater/porewater and the precipitation of siliceous polymorphs did not took
422 place. The similar state of siliceous sponge fossil preservation, but containing only ferrigenous
423 coatings of limonite group (Fig. 5f), is also documented in opoka sections, however, in the last
424 the silica polymorphs (as opal-CT) are present in the rock matrix, as well as significant amount
425 of newly formed calcite (Jurkowska, 2022). This suggests that in the upper Turonian limestone,
426 although the siliceous skeletons undergo dissolution, cherts and opoka did not form due to the
427 existence of a factor, that limits silica polymorphs precipitation. Taking into account that during



428 the Cretaceous the seawater dSi concentration was high (Siever, 1991), the diminished rate of
429 calcium carbonate dissolution (due to small amount of OM) and the related lack of available
430 alkalinity and Mg^{2+} ions could be the cause of the lack of a new silica polymorph precipitates
431 (Williams and Crerar, 1985; Kastner et al., 1977). The latter is a very probable factor because
432 the time intervals of Turonian calcisphere blooms are correlated with events of unusually high
433 Ca^{2+} concentration and low Mg/Ca ratio (Stanley et al., 2005; Van Dijk et al., 2016; Ciurej et
434 al., 2023) which could limit the availability of Mg^{2+} ions essential for silica polymorphs
435 precipitation (Williams and Crerar, 1985; Kastner et al., 1977). Another factor that needs to be
436 taken into account is lower dSi seawater concentration, which could occur in some areas during
437 the Cretaceous (Jurkowska and Świerczewska-Gładysz, 2020a), but this aspect has never been
438 studied in Turonian limestone. The very abundant hexactinellid sponges documented in
439 Turonian limestone are similar to those noted in Campanian opoka deposited under relatively
440 high dSi seawater concentration (Jurkowska and Świerczewska-Gładysz, 2022) which
441 contradicts the diminished seawater dSi concentration during time of Turonian limestone
442 deposition and implies that similar conditions could have existed during the limestone
443 formation. The presence of pyrite and ferrigenous coatings only in a microenvironment
444 outlining the previous siliceous sponge skeleton and their absence in the surrounding mud is
445 also related to the presence of OM and its distribution within the sponge body. Although the
446 general content of OM in studied rocks is small, observation indicate that the OM is preserved
447 as lumps of homogeneous mass or fibrous texture associated only with sponge skeletons (Fig.
448 5f) and always occurs with pyrite crystals/limonite coatings. This association, which is quite
449 common in the paleontological record, is usually connected with distinctive reductive
450 conditions and acidic pH created by bacterial decomposition of OM in a small
451 microenvironment surrounding the organism remnants. Those characteristic conditions are
452 different from the geochemical conditions of the environment in the surrounding mud.



453 Comparing the preservation of siliceous sponge skeleton as ferrigenous coatings from opoka
454 (Fig. 3f-i) and limestone, the difference is attributed to the variable mineral phases that build
455 those coatings. In opoka, the siliceous sponge skeleton outline is formed of the limonite group
456 (Fig. 3f-i), while in limestone, pyrite crystals partially covered by limonite mass occur (Fig. 5c,
457 d), indicating that in the former, the oxic conditions prevailed during iron minerals formation,
458 while in the second the anoxic conditions prevailed. The oxidation pitches and dissolution
459 features visible on pyrite euhedral crystals (Fig. 5e), indicate a later oxidation event, which
460 could also cause the transformation of pyrite into limonite group minerals. This could be
461 connected with recent conditions, probably occurring during rock excavation or during late
462 diagenesis due to contact with oxygenated porewater.

463 In limestone, the presence of OM associated only with siliceous sponges (Fig. 5f) and with
464 pyrite mineralogy indicates that due to oligotrophic conditions, the OM underwent anaerobic
465 microbial decomposition, while not decaying in an oxic zone. This is caused by the relatively
466 small number of sponge-feeding predators (e.g. specialized snails, starfish) (e.g. Stratmann et
467 al., 2022; López-Acosta et al., 2023). Additionally, under oligotrophic conditions, the rare
468 bottom-feeding organisms did not facilitate the sponge fragmentation. In the studied
469 environment, because of oligotrophic conditions, this process took place deeper within the
470 sediment column in the dysoxic/anoxic iron and sulphate reduction zone, where the pyrite was
471 formed due to availability of the essential substrates (Fe^{2+} and H_2S) for its precipitation.

472 In the opoka environment, in which the oxic and eutrophic conditions prevailed, the OM on a
473 sponge body decomposed in an oxic zone, causing that iron oxides and hydroxides the
474 formation (Fig. 3f-h).

475 The formation of pyrite crystals, as well as limonite group minerals, needs iron availability in
476 the immediate vicinity of the sponge skeleton in an amount higher than its content in seawater.

477 The presence of a significant amount of iron (Fe^{2+}) essential for the formation of iron sulphides



478 (pyrite) and iron oxides/hydroxides around the sponge remnants could be associated with the
479 organism's biomineralization process during which the iron was actively accumulated in a
480 living sponge body (Gentric et al., 2016; Kubiak et al., 2023). The silanol groups (Si-OH) of
481 siliceous sponges can also bond Fe^{2+} to the structure by replacement of OH groups. The Fe^{2+}
482 (Ferretti et al., 2019) is released during siliceous skeleton dissolution and saturates the
483 microenvironment. Moreover, observations of modern sponges have shown that the skeletons
484 of dead sponges, as a result of long-term contact with seawater/porewater, become covered with
485 a coating containing metal ions, including iron ions, which are incorporated in into structure of
486 amorphous silica (Hurd 1973; Chu et al., 2011). These iron ions come from seawater/porewater
487 and are attracted by the negatively charged surface occurring on the silica sponge framework.

488

489 *5.3.2 The OM content in a closed microenvironment of the decaying sponge body*

490 The state of siliceous sponge preservation in the upper Turonian-lower Coniacian marls is
491 significantly different from that observed in the limestone (Chapter 5.3.1), which is caused by
492 the formation of a geochemically different, closed microenvironment inside the decaying
493 sponge compared to the surrounding sediment. Trapped OM within the sponge came from
494 sponge's body, microbes decomposing it, and also from their symbiotic microbes (Kluijve et
495 al. 2021) and microbes that decompose the sponge's body (Stratmann et al. 2022). Within the
496 state of preservation of sponge skeletons from these marls, the two types related to sponge
497 groups, their morphology, and distribution of OM within the spaces in the skeleton could be
498 distinguished: (1) the rigid (choanosomal) skeleton of hexactinellid and lithistid sponges
499 preserved as pyrite infillings with marcasite (Fig. 3a, b; 6a) and barite (only in lithistids) (Fig.
500 6b) and the surface part of the skeleton (loose ectosomal spicules and/or external choanosomal
501 network) preserved as siliceous (Fig. 3c, 6b); (2) the loose spicules of body-preserved non-rigid
502 demosponges with dissolved siliceous skeleton occurring as pyrite and marcasite infillings



503 associated with barite (Fig. 3b, 6c, e, g, h). The typical feature of both these types of
504 preservation is the presence of carbonate sediment occurring inside the spaces between spicules
505 (loose, articulated, or fused) in the form of authigenic small grains of homogeneous
506 coalescence/fused texture (Fig. 6d) and large sparite crystals forming cements (Fig. 6e). These
507 texture were formed due to complete primary calcite dissolution followed by its reprecipitation
508 in the sediment infilling the sponges. Such authigenic grains were not documented in the
509 surrounding carbonate mud (Fig. 6f), indicating that the closed microenvironment must have
510 developed inside the decomposing sponge body and governed geochemical conditions different
511 from those in the surrounding environment. The formation of a closed microenvironment cut
512 off from surrounding porewater probably started before sponge burial and was generated by
513 microbial biofilm formed around the decaying sponge remnants (compare Stratmann et al.,
514 2022) (Fig. 7). After burial, the chemical barrier between the decaying sponge and surrounding
515 sediment was also facilitated by the high clay content within the seabed mud, which formed a
516 physical barrier (Fig. 6f).

517 In both types of preservation, the anoxic and acidic pH conditions generated inside the sponge
518 body due to OM decomposition and cutting off from external oxic environment trigger the
519 dissolution of opal-A in sponge spicules and crystallization of small euhedral pyrite crystals in
520 space between spicules, as well as the precipitation of massive polycrystalline pyrite infillings
521 in voids left after spicules (Fig. 3a, b, 6a, g-i) (compare Reolid, 2014) (Fig. 7). Although all
522 factors necessary for silica polymorphs precipitation were available inside the sponge, it did not
523 precipitate due to a too low dSi concentration, indicating that the dSi concentration generated
524 by sponge spicules dissolution was not high enough to initiate the silica polymorphs
525 crystallization. The pyrite precipitation took place under euxinic conditions in the presence of
526 Fe²⁺ ions, which were produced during OM decomposition by iron-reducing bacteria, followed
527 by H₂S production by bacterial sulphate reduction. These distinctive geochemical conditions



528 led to pyrite precipitation as the first stable iron sulfide in the form of massive polycrystalline
529 textures under low Eh (Grimes et al., 2002) (Fig. 6g-i), generated inside the voids left after
530 spicules dissolution, simultaneously with its precipitation as octahedral crystals within the
531 sediment infilling the spaces between spicules, under the lower Eh than in spicules (Fig. 7). In
532 the studied samples, the EBSD studies revealed that marcasite is present in the form of euhedral
533 crystals in the sediment matrix (Fig. 6h, i), usually in areas surrounding the spicules and also
534 associated with pyrite building its infillings (Fig. 6h, j). Although the acid conditions generated
535 by OM decomposition favors the pyrite precipitation (pH ~ 6), they were simultaneously
536 buffered by calcite complete dissolution, which was a limiting factor for marcasite
537 precipitation (in pH ~4–5; Schoonen and Barnes, 1991; Murowchick and Barnes, 1987;
538 Benning et al., 2000). The marcasite precipitation took place via the oxidation of previously
539 formed pyrite (Scheiber et al., 2007) (Fig. 7). This process provided the Fe^{2+} , facilitate the pH
540 decrease to a level enabling marcasite formation, and simultaneously increased further calcite
541 dissolution. The presence of marcasite indicates that the redox shift occurred, probably due to
542 intrusion of the oxygenated porewater into the previously closed environment of the decaying
543 sponge body. Taking into account that marcasite precipitation is a much faster process than
544 pyrite formation (Schoonen and Barnes, 1991), the oxidation events were rapid and probably a
545 repeated process. The intrusion of porewater was possible due to ongoing process of OM
546 decomposition and siliceous skeleton dissolution, which created a system of holes and
547 passageways enabling porewater penetration. Barite (BaSO_4) infills the voids left after central
548 canal dissolution (Fig. 3b, 6g, h) and occurs in form of the patches of loosely arranged crystals
549 fused into one mass, usually associated with large (100–150 μm) sparite crystals (Fig. 6c, e).
550 This distinctive barite distribution was controlled by its formation, which was governed by the
551 presence and distribution of OM and availability of SO_4^{2-} under oxic conditions (Liguori et al.,
552 2016). The latter was easily available in the solution due to marcasite formation via pyrite



553 oxidation, which provide the SO_4^{2-} (Scheiber, 2007), while the remnants of dissolved OM in
554 the central canal of the sponge spicule and lumps of OM surrounding the sponge skeleton acted
555 as an nucleation sites due to the presence an amorphous P-phase precursor, which binds the Ba
556 and promotes its high concentration essential for barite precipitation (Martinez-Ruiz et al.,
557 2020) (Fig. 7). The lack of barite within the remains of hexactinellids with rigid skeleton was
558 the result the small amount of OM related to the construction of these sponges, preventing barite
559 precipitation. After the decomposition of OM declined, the pH increased, and in a laying deeper
560 in the sediment sulphate reduction zone reached the level of > 7.8 , enabling the calcite
561 reprecipitation in the form of authigenic small grains fused into homogenous coalescence/fused
562 texture and large sparite crystals forming cements (Fig. 6e). The distribution of the sparite
563 cements indicates that the presence of remnants of OM within the sediment, highlighted by
564 barite precipitation, were the preferential areas for newly formed sparite crystal growth due to
565 highly alkaline pH (~ 12) conditions generated by sulphate reduction bacteria, which controlled
566 the distinctive microtexture of the calcite. The presence of authigenic calcite grains of
567 distinctive microtexture only in sediment infilling the sponge (not in the surrounding sediment)
568 indicates that although the sponge remnants at that stage did not form a closed
569 microenvironment, but rather semi-closed one, the diagenetic transformations were different
570 from those in the surrounding sediment. This situation was caused by the presence of a
571 significant amount of detrital clays (up to 16% vs. 11% in sediment) only in the sediment
572 surrounding the sponge remnants. Moreover, the presence of clays retards the silica dissolution
573 (Kastner et al., 1977), leading to longer preservation of surfaces parts of sponge siliceous
574 skeleton that were in contact with the sediment (type 1). The clays also play an important role
575 as a dSi sink during diagenetic clay transformations (Fig. 6f), indicating that the dSi provided
576 by siliceous skeleton dissolution was absorbed by the clays, leading to a decline in the dSi
577 concentration, which prevented the opal-CT precipitation.



578 The geochemically distinct closed microenvironment forming inside the decaying sponge is
579 also rarely noted in opoka. In this lithology, the siliceous infillings of skeletal elements (of
580 mixed opal-CT and nano- α -quartz) occur occasionally, mainly in lithistids (Fig. 3j)
581 (Świerczewska-Gładysz, 2006). The closed microenvironment, which established around the
582 decaying sponge body, formed a chemical barrier for the dSi migration to the outside seabed
583 mud, causing in situ authigenic silica precipitation (Jurkowska and Świerczewska-Gładysz,
584 2020a). This distinctive microenvironment inside the dead sponge was created by microbial
585 decomposition of OM, which were trapped and protected from the organisms penetrating the
586 mud by dysoxic/anoxic conditions that stabilized inside the decaying sponge body. In samples
587 of bodily preserved hexactinellids with rigid skeleton, small fragments of the skeletal network
588 preserved as silica are extremely rare and consists of relatively large spicules (Świerczewska-
589 Gładysz, 2006). These sponges, due to their morphology (thin wall) did not create a close
590 microenvironment, and the skeletons are dissolved and infilled by ferruginous mass of the
591 limonite group (Fig. 3 f-h). Thus, the presence of OM itself was not a factor that control the
592 silica authigenic precipitation of nano- α -quartz and lepispheric opal-CT, and only hindered the
593 outflow of dissolved silica from the sponge skeleton to porewater.

594

595 *5.3.3 Third factor: the impact of the mineralogical composition of the seabed mud on dSi*
596 *precipitation*

597 The mineralogical composition of the seabed mud may affect silica polymorph precipitation in
598 two main ways: by scavenging the dSi through clays during its diagenetic transformations or
599 by limiting the Mg^{2+} availability, for example, due to decreased calcite dissolution (during the
600 pH drop the high-Mg calcite undergoes dissolution first). In the studied rocks, clays are
601 significant within two lithologies: of upper Turonian-lower Coniacian and lower-middle
602 Campanian marls, in which their average content is 11% and 20%, respectively (Jurkowska,



603 2022). In both lithologies, the clays are mostly of detrital origin, but during diagenesis, they
604 undergo transformation, which is visible in their microtexture (Garrels and MacKenzie, 1967;
605 Siever and Woodford, 1973; Isson and Planavsky, 2018; Jurkowska, 2022). During these
606 transformations, the clays consume the dSi, Al (alkali metal cations), and alkalinity, and the
607 whole process is controlled by the availability of essential substrates, pH and fluid temperature
608 (Siever and Woodford, 1973). It has been experimentally revealed that, in seawater and
609 porewater under a relatively stable pH ~8, the sorption and dissolution reactions of various clay
610 minerals are dependent on dSi concentration. Generally, for illite/smectite, which is the most
611 common clay mineral, the dSi concentration at the sorption point starts at 25 ppm (250 μ M),
612 while the kinetic sorption equilibrium for clay minerals is estimated to be approximately 60
613 ppm (1000 μ M) (Siever and Woodford, 1973; Siever, 1991). The range of dSi concentration
614 (25–60 ppm) overlaps with the dSi concentration favourable for silica polymorph precipitation
615 (Mackenzie and Gees, 1971; Williams and Crerar, 1985), which indicates that during early
616 diagenesis within the seabed mud, a dynamic equilibrium between these two mineral phases
617 must have existed.

618 In the studied upper Turonian-lower Coniacian marls, the balance stabilized at a level that
619 enabled the precipitation of secondary silica polymorphs only in the external part of the
620 siliceous sponge skeleton (while the internal spicules underwent dissolution and the voids were
621 infilled by different minerals) (Fig. 3c; 6a-c). In the lower-middle Campanian marls, the
622 precipitation of silica polymorphs took place not only as infillings of loose siliceous spicules
623 and skeletal networks (in the form of mixed nano- α -quartz and opal-CT (Fig. 8a-b), but also
624 within the sediment in the form of opal-CT lepispheres (Fig. 8c). Taking into account that
625 overall dSi seawater concentration was similar during the formation of both types of marls and
626 was at the level of opal-CT (25–60 ppm) (Siever, 1991), this indicates that the formation of
627 silica polymorphs (also cherts) is also dependent on the chemical equilibrium within the seabed



628 mud. This can lead to a situation in which, although the siliceous sponges underwent
629 dissolution, silica polymorphs precipitation would not be initiated. The observed mineralogical
630 variability in marls could also be explained by a higher overall dSi seawater concentration noted
631 in the Campanian (Jurkowska and Świerczewska-Gładysz, 2020a, b) compared to the
632 diminished dSi concentration in the Turonian-lower Coniacian. Under lower dSi concentration,
633 clays will be the preferential minerals that absorb dSi.

634

635 **6. Discussion**

636 *6.1 The role of siliceous sponges as a main source of dSi in a porewater and dSi burial from* 637 *a geological perspective*

638 In geological studies, the precipitation of cherts and authigenic silica polymorphs was treated
639 as a reflection of a significant amount of dSi delivered by the dissolution of siliceous sponge to
640 porewater, which enables the precipitation of opal-CT (Wise and de Weaver, 1974; Jeans, 1978;
641 Clayton, 1984, 1986; Maliva and Siever, 1989a, b; Maliva et al., 1989). The model of siliceous
642 chert formation presented by Siever (1986) assumes that its main mechanism was dSi
643 downward diffusion between seawater and porewater, which was driven by the higher
644 porewater dSi concentration generated by the dissolution of siliceous sponges. Unfortunately,
645 in many later works, although they are based on Siever (1986) mechanisms of chert formation,
646 the oversimplification of this mechanism led to the assumption that dSi diffusion occurred only
647 between the dissolving siliceous sponges and sediment mud, while the role of seawater dSi
648 concentration was completely ignored (Wise and de Weaver, 1974; Jeans, 1978; Clayton, 1984,
649 1986; Maliva and Siever, 1989a, b; Maliva et al., 1989). This simplification led to the
650 straightforward conclusion that the dissolution of siliceous sponges controls the porewater dSi
651 concentration and was the main source of dSi, governing its burial in the form of siliceous rocks.
652 The role of seawater as a source of dSi, even that during the Palaeozoic and Mesezoic, when its



653 concentration was estimated to be high (at the level of opal-CT; Siever, 1991), is interpreted as
654 insignificant (Maliva and Siever, 1989a, b). The results presented here indicate that although
655 the process of siliceous sponge skeleton dissolution was common in deposits of Cretaceous
656 seas, the role of the bSi (biogenic silica) inflow generated by this process in controlling dSi
657 concentration and as a source for silica polymorph precipitation was subordinate, while most
658 of the siliceous rocks were formed due to dSi downward diffusion from seawater to porewater
659 (Jurkowska and Świerczewska-Gładysz, 2020a, b). As documented here, the presence of
660 abundant siliceous sponges (Turonian-upper Coniacian marls) which were buried did not
661 determine the precipitation of silica polymorphs under conditions of lower dSi concentration in
662 porewater (related to low dSi concentration in seawater and/or the absorption of dSi by clay
663 minerals), which probably occurred during this time. Similarly, preserved rigid skeletons or
664 loose spicules of siliceous sponges as voids infilled by iron minerals are common in the fossil
665 record (of Paleozoic and Mesozoic calcareous and detrital rocks) in which cherts are absent
666 (e.g. Rigby et al., 1995; Vodrážka, 2009; Xiao et al., 2005; Madsen et al., 2010; Reitner, 2013;
667 Reolid, 2014). This pattern has also been confirmed in review studies by the authors on
668 Palaeozoic cherts, which show that facies distribution during that time did not correlate with
669 siliceous sponge occurrences but is associated with dSi inflow via the volcanic-hydrothermal
670 activity connected with LIP (Large Igneous Provinces) (literature review in Jurkowska and
671 Świerczewska-Gładysz, 2024).

672 The presence of fossils of siliceous sponges in siliceous rock cannot be treated as a direct
673 argument for the biogenic origin of siliceous and carbonate-siliceous rocks, since the
674 fossilization process depends on many environmental factors. The studies presented here, based
675 on mineralogical and microtextural observations, indicate that the process of dSi migration
676 occurring after the dissolution of siliceous sponge skeletons was driven by the interaction
677 between different sites (siliceous sponge remains, newly forming silica polymorphs of opal-



678 CT) controlling the dynamic equilibrium of dSi concentration, which governs the dissolution
679 and precipitation of silica. The observed association of occurrence of siliceous sponges within
680 cherts and opoka (Wise and de Weaver, 1974; Jeans, 1978; Clayton, 1984, 1986; Maliva and
681 Siever, 1989a, b) could be explained by the fact that basin areas characterized by significant
682 amount of dSi inflows were preferentially settled by silicifiers due to the availability of the main
683 substrate for building their skeletons. Moreover, the studies presented indicate that under high
684 seawater dSi concentration (as noted during the Campanian cherts formation), due to secondary
685 infilling of the voids left after siliceous sponge dissolution and the preservation of voids after
686 spicules, the fossils of siliceous sponges have higher preservation potential, which could also
687 affect the observations and lead to simplified conclusions.

688

689 *6.2 The role of seawater dSi concentration in Si circulation and burial*

690 The evolution of the Si cycle in Earth's history and the associated fluctuations of dSi seawater
691 concentrations have been presented in the classical studies by Maliva and Siever (1989a, b) and
692 Siever (1991). The seminal model assumes that the overall seawater dSi concentration was
693 relatively stable and high for most of the Palaeozoic and Mesozoic times, reaching the level of
694 opal-CT precipitation (250–700 μm), which is much higher than today's, which is below quartz
695 precipitation ($< 250 \mu\text{M}$). Our previous studies indicate that during the Cretaceous, in the
696 marine environment of the epicontinental European Basin, the seawater dSi concentration was
697 not stable and only in some areas reached the higher concentrations enabling the precipitation
698 of silica polymorphs (Jurkowska and Świerczewska-Gładysz, 2020a, b). Similarly, the studies
699 by Doering et al. (2024) indicate that during the Cretaceous, the dSi concentration of sea bottom
700 water was much lower than assumed in classical model (Maliva and Siever, 1989a; Siever,
701 1991).



702 The research conducted here indicates that the formation of cherts and the precipitation of silica
703 polymorph within the seabed mud are controlled by the seawater dSi concentration, which via
704 dSi downward diffusion to the porewater. In the studied Turonian-upper Coniacian section,
705 silica polymorphs did not precipitate in the seabed mud (neither as cherts nor as opoka), even
706 in the presence of biogenic dSi from siliceous sponges. Among the factors that could prevent
707 the precipitation of silica polymorphs, low seawater dSi concentration (lower than assumed for
708 the Cretaceous) is very probable. Even if downward dSi diffusion between seawater and
709 porewater occurred and dSi input from the dissolution of siliceous sponges was also added to
710 porewater, dSi concentration was still too low to initiate the precipitation of silica polymorphs.
711 Unfortunately, the lack of authigenic silica polymorphs in the rocks makes it impossible to
712 perform analyses that could verify this hypothesis.

713

714 *6.3 The $\delta^{30}\text{Si}$ signatures from fossilized sponges skeletons*

715 The isotopic analysis of $\delta^{30}\text{Si}$ is widely used as a paleoceanographic and paleoproductivity
716 proxy in marine studies to constrain the Si cycle and reconstruct of past seawater dSi
717 concentrations (De La Rocha et al., 1997, 1998; Sutton et al., 2018; Farmer et al., 2021). In the
718 geological record, the materials used for $\delta^{30}\text{Si}$ measurement are siliceous rocks, mainly cherts
719 (e.g. Van der Boorn et al., 2007; 2010; Tatzel et al., 2015; Gao et al., 2020), and remnants of
720 the skeleton of silicifiers (diatoms, sponges, radiolarians) in sub-fossil and fossil states (e.g.
721 Egan et al., 2012; Fontorbe et al., 2017; 2020). The main limitations in using this tool for the
722 interpretation of paleorecords is dictated by the necessity of siliceous remnants that are built of
723 original biogenic opal-A, free from contaminating sources (Sutton et al., 2018). This kind of
724 fossil and subfossil material is very rare in the geological record (especially in rocks older than
725 the Paleogene) due to diagenetic changes of silica polymorphs occurring after burial. The data
726 presented in these studies indicate that in Cretaceous and older deposits (Palaeozoic and



727 Mesozoic; Jurkowska and Świerczewska-Gładysz, 2024), the siliceous remains of sponge
728 skeletons are built of secondary opal-CT, and this is the main common state of their preservation
729 (Jurkowska and Świerczewska-Gładysz, 2020a). This strongly limits the possibility of using
730 $\delta^{30}\text{Si}$ as a paleoceanographic proxy or for the estimation of seawater dSi concentration (Wille
731 et al., 2010; Hendry et al., 2012) on older paleontological material. Only single measurements
732 of $\delta^{30}\text{Si}$ on preserved original biogenic opal-A silicifiers older than the Eocene were performed
733 due to the scarcity of suitable material (Cassarino et al., 2024; Doering et al., 2024). Although
734 this exceptionally well-preserved material provides important data on seawater dSi
735 concentration during the Cretaceous, it represent only fragmented part of the whole system.
736 On one side, the data presented here constrain the use of $\delta^{30}\text{Si}$ of fossil material as an ad hoc
737 paleorecord proxy, but on the other side, the presented diagenetic models indicate that the $\delta^{30}\text{Si}$
738 of secondary infilled sponge skeletons could potentially carry signals indicating the dSi origin
739 (seawater or hydrothermal) (Fig. 4). The main questions that arises is about the share of
740 individual sites (which according to the diagenetic model are mainly dSi from seawater and bSi
741 from siliceous sponges) in the dSi of porewater from which silica polymorphs precipitation
742 took place, and also about the Si isotope fractionations that can occur during the process of
743 opal-CT precipitation followed by its later maturation within the same polymorphic phase.
744 In many works, the $\delta^{30}\text{Si}$ of cherts has been used for to recognize the dSi source (seawater or
745 hydrothermal), although it must be highlighted that this method is certainly valid for the
746 Precambrian and Cambrian cherts (Van der Boorn et al., 2007; 2010; Tatzel et al., 2015; Gao
747 et al., 2020), which were formed before siliceous sponge became an important part of the Si
748 cycle (Jurkowska and Świerczewska-Gładysz, 2024). During that time, due to the insignificant
749 role of silicifiers in Si cycle, the seawater–porewater system could be treated as closed, and the
750 $\delta^{30}\text{Si}$ signatures reflect the isotope fractionation occurring between the dSi source (volcano-
751 hydrothermal) and authigenic silica polymorph precipitation during diagenesis. Unfortunately,



752 in many works, cherts are used as an ad hoc paleoceanographic proxy without considering Si
753 isotope fractionation by silicifiers and the diagenetic impact of occurring silica polymorph
754 transformation. More studies based on the model presented here (and in previous works:
755 Jurkowska and Świerczewska-Gładysz, 2020a, b) of dSi migration and diffusion are needed to
756 recognize how the Si isotopes fractionate during diagenesis and what $\delta^{30}\text{Si}$ signature studies of
757 secondary silica polymorphs reflects.

758

759 **7. Conclusions**

760 The conducted research revealed that the process of siliceous sponge dissolution within the
761 Cretaceous marine environment of the epicontinental basin commonly occurred in the seabed
762 mud and in small amount saturated the porewaters with dSi. The later occurring authigenic
763 silica polymorph precipitation within the seabed mud (the formation of chert and other
764 siliceous/carbonate-siliceous rocks) depended on environmental factors such as: overall OM
765 content (which, by microbial decomposition, triggered the geochemical changes facilitating
766 opal-CT precipitation), and the mineralogical composition of the seabed mud (in terms of the
767 presence of minerals that deliver essential alkalinity – carbonates – and those that scavenge the
768 dSi – clays). Although these agents were important, the dSi seawater concentration was the
769 main controlling factor of porewater dSi concentration due to constant diffusion and dSi
770 migration. The dynamic equilibrium of seawater-porewater dSi concentration governs the
771 precipitation of silica polymorphs in sediment and in voids left after spicules dissolution. High
772 seawater dSi concentration is recorded in the geological succession by the occurrence of cherts
773 and opoka, while its low concentration is reflected by the absence of these rocks, even in the
774 sections in where siliceous sponges are abundant and represented by remains with completely
775 dissolved primary skeleton. In these sections, the decaying sponge body often formed a closed
776 microenvironment characterized by different geochemical conditions compared to the



777 surrounding mud, which is visible in the geological record as the common preservation of
778 sponge skeletal remnants as pyrite/marcasite infillings or in the form of limonite coatings. The
779 skeletons of fossil sponges that are preserved as siliceous are in fact secondary infilled by
780 authigenic silica polymorphs (mixed nano- α - quartz and opal-CT), which limits the usefulness
781 of $\delta^{30}\text{Si}$ as paleoceanography proxy in geological studies but highlights its utility for the
782 identifying dSi origin and estimating dSi concentration.

783

784 **Data availability**

785 All raw data can be provided by the corresponding author upon request. The rock samples and
786 paleontological samples of siliceous sponges are stored at AGH University.

787 **Author contributions**

788 AJ and EŚG contributed to the idea, conceptualization and wrote the manuscript draft. AJ
789 conducted the mineralogical and microtextural studies of rocks and fossils and data
790 interpretations. EŚG worked on the taxonomy of fossils of sponge remains, and fossils sample
791 collections and selection. SzKF edited the manuscript, made language corrections, and prepared
792 samples for analysis.

793 **Competing interests**

794 The authors declare that they have no conflict of interest.

795 **Acknowledgements**

796 Many thanks go to Adam Gaweł (AGH) for valuable help with SEM-EDS analysis and to Dr.
797 Grzegorz Cios (AGH Academic Center for Materials and Nanotechnology) for support with
798 EBSD analysis.

799 **Financial support**

800 This research project is supported by program „Excellence initiative – research university” for
801 the AGH University.



802 **Literature**

- 803 Alexandrowicz, S.W. and Radwan, D.: Kreda opolska - problematyka stratygraficzna i
804 złożowa, *Przegląd Geologiczny*, 20, 183–188, 1973.
- 805 Benning, L.G., Wilkin, R.T. and Barnes, H.L.: Reaction pathways in the Fe-system below
806 100uC, *Chem. Geol.*, 167, 25–51, 2000.
- 807 Bertolino, M., Calcinai, B., Cattaneo-Vietti, R., Cerrano, C., Lafratta, A., Pansini, M., Pica, D.
808 and Bavestrello, G.: Stability of the sponge assemblage of Mediterranean coralligenous
809 concretions along a millennial time span, *Mar. Ecol.*, 35, 149–158, 2013.
- 810 Bertolino, M., Oprandi, A., Santini, C., Castellano, M., Pansini, M., Boyer, M., Bavestrello,
811 G.: Hydrothermal waters enriched in silica promote the development of a sponge community
812 in North Sulawesi (Indonesia), *The Eur. Zoo. J.*, 84(1), 128–135, 2017.
- 813 Bieda, F.: Sur les spongiaires siliceux du Sénonien des environs de Cracovie, *Rocznik
814 Polskiego Towarzystwa Geologicznego*, 9, 1–41, 1933.
- 815 Bromley, R.G. and Ekdale, A.A.: Trace fossil preservation in flint in the European Chalk, *J.
816 Paleontol.*, 58(2), 298–311, 1984.
- 817 Calvert, S.E.: Deposition and diagenesis of silica in marine sediments, in: Hsü, K.J. and
818 Jenkyns, H.C. (Eds.), *Pelagic Sediments: On Land and under the Sea*. Sp. Pub. Int. Assoc.
819 *Sedimentologists*, 1, 273–299, 1974.
- 820 Calvert, S.E.: Mineralogy of silica phases in deep-sea cherts and porcelanites, *Mar. Mineral.
821 Philos. Transac. Royal Soc. A*, 286, 239–252, 1977.
- 822 Cassarino, L., Brylka, K., Dai, Y., Pickering, R.A., Richoz, S., Conley, D.J.: What we can
823 learn from the oldest and first $\delta^{30}\text{Si}$ diatom taxa specific record? In *Abstracts of Isotopes in
824 Biogenic Silica (IBiS)*, 3, 2024.
- 825 Chu, J.W.F., Maldonado, M., Yahel, G. and Leys, S.P.: Glass sponge reefs as a silicon sink,
826 *Mar. Ecol. Prog. Ser.*, 441, 1–14, 2011.
- 827 Ciurej, A., Dubicka, Z. and Poberezhsky, A.: Calcareous dinoflagellate blooms during the
828 Late Cretaceous ‘greenhouse’ world - a case study from western Ukraine, *PeerJ*, 11, e16201
829 <http://doi.org/10.7717/peerj.16201>, 2023.
- 830 Clayton, C.J.: *Geochemistry of Chert Formation in Upper Cretaceous Chalk*, PhD Thesis.
831 University of London, 1984.
- 832 Clayton, C.J.: The chemical environment of flint formation in Upper Cretaceous Chalks, in:
833 de Sieveking, G. and Hart, M.B. (Eds.), *The Scientific Study of Flint and Chert*, P. Fourth Int.
834 *Flint Symp. Held at Brighton Polytechnic*, 10–15 April 1983. Cambridge University Press,
835 Cambridge, 43–54, 1986.
- 836 Costa, G., Bavestrello, G., Cattaneo-Vietti, R., Dela Pierre, F., Lozar, F., Natalicchio, M.,
837 Violant, D., Pansini, M., Rosso, A. and Bertolino, M.: Palaeoenvironmental significance of
838 sponge spicules in pre-Messinian crisis sediments, Northern Italy, *Facies*, 67, 9, 2021.



- 839 De La Rocha, C. L., Brzezinski, M. A., and DeNiro, M. J.: Fractionation of silicon isotopes by
840 marine diatoms during biogenic silica formation, *Geochim. Cosmochim. Acta*, 61(23), 5051–
841 5056, 1997.
- 842 De La Rocha, C. L., Brzezinski, M. A., DeNiro, M. J., and Shemesh, A.: Silicon isotope
843 composition of diatoms as an indicator of pastoceanic change, *Nature*, 395, 680–683, 1998.
- 844 Dias-Brito, D.: Global stratigraphy, palaeobiogeography and palaeoecology of Albian–
845 Maastrichtian pithonellid calcispheres: impact on Tethys configuration, *Cretaceous Res.*, 21,
846 315–349, 2000.
- 847 Doering, K., Zhang, Z., Dai, Y., Dummann, W., Störling, T., Schröder-Adams, C., Richoz, S.,
848 Frank, M., Herrle, J., Harwood, D., Conley, D.J.: The silica cycle during the Upper
849 Cretaceous: the case study from Canadian Continental Shelf. In *Abstracts of Isotopes in*
850 *Biogenic Silica (IBiS)*, 8, 2024.
- 851 Egan, K. E., Rickaby, R. E. M., Leng, M. J., Hendry, K. R., Hermoso, M., Sloane, H. J.,
852 Bostock, H. and Halliday, A.N.: Diatom silicon isotopes as a proxy for silicic acid utilisation:
853 A Southern Ocean core top calibration, *Geochim. Cosmochim.*, 96, 174–192, 2012.
854 <https://doi.org/10.1016/j.gca.2012.08.002>, 2012.
- 855 Farmer, J. R., Hertzberg, J. E., Cardinal, D., Fietz, S., Hendry, K., Jaccard, S. L., Paytan, A.,
856 Rafter, P.A., Ren, H., Somes, C.J. and Sutton, J.N.: Assessment of C, N, and Si isotopes as
857 tracers of past ocean nutrient and carbon cycling, *Global Biogeochemical Cy.*, 35,
858 e2020GB006775. <https://doi.org/10.1029/2020GB006775>, 2021.
- 859 Ferretti, A., Messori, F., Di Bella, M., Sabatino, G., Quartieri, S., Cavalazzi, B., Italiano, F.
860 and Barbieri, R.: Armoured sponge spicules from Panarea Island (Italy): Implications for their
861 fossil preservation, *Palaeogeogr. Palaeoecol.*, 536, 109379,
862 <https://doi.org/10.1016/j.palaeo.2019.109379>, [2019](#).
- 863 Fontorbe, G., Frings, P. J., De La Rocha, C. L., Hendry, K. R., Carstensen, J., and Conley, D.
864 J.: Enrichment of dissolved silica in the deep Equatorial Pacific during the Eocene-Oligocene,
865 *Paleoceanography*, 32(8), 848–863, 2017.
866
867 **Fontorbe, G., Frings, P.J., De La Rocha, Ch.L., Hendry, K.R. and Conley,**
868 **D.J.:** Constraints on Earth System Functioning at the Paleocene-Eocene Thermal Maximum
869 From the Marine Silicon Cycle, *Paleoceanography and Paleoclimatology*, **35**, **5**,
870 <https://doi.org/10.1029/2020PA003873>, 2020.
- 871 Gao, P., Li, S., Lash, G.G., He, Z., Xiao, X., Zhang, D. and Hao, Y.: Silicification and Si
872 cycling in a silica-rich ocean during the Ediacaran-Cambrian transition, *Chem. Geol.* 552,
873 119–789, 2020.
- 874 Garrels, R.M. and Mackenzie, F.T.: Origin of the Chemical Compositions of Some Springs
875 and Lakes (ed. Stumm W.) *Equilibrium concepts in natural water systems [J]*, *J. Am.*
876 *Chemical Soc.*, 222–242, 1967.
- 877 Gentric, C., Rehel, K., Dufour, A. And Sauleau, P.: Bioaccumulation of metallic trace
878 elements and organic pollutants in marine sponges from the South Brittany Coast, France, J.



- 879 Environ. Sci. Heal. A, 51(3), 213–219, <https://doi.org/10.1080/10934529.2015.1094327>,
880 2015.
- 881 Grimes, S.T., Davies, K.L., Butler, I.B., Brock, F., Edwards, D.R., Richard, Briggs, D.E.G.
882 and Parkes, R.J.: Fossil plants from the Eocene London clay: the use of pyrite textures to
883 determine the mechanism of pyritization, *J. Geol. Soc. London*, 159, 493–501, 2002.
- 884 Heath, G.R. and Moberly Jr., R.: Cherts from the western Pacific, leg 7, Deep Sea Drilling
885 Project, in: Winterer, E.L., Riedel, W.R., et al. (Eds.), *Initial Rep. Deep Sea, 7. U.S.*
886 *Government Printing Office, Washington*, 991–1007, 1971.
- 887 Hendry, K.R. and Robinson, L.F.: The relationship between silicon isotope fractionation in
888 sponges and silicic acid concentration: Modern and core-top studies of biogenic opal,
889 *Geochim. Cosmochim. Ac.*, 81, 1–12, 2012.
- 890 Hurcewicz, H.: Siliceous sponges from the Upper Cretaceous of Poland, Part I, Tetraxonia,
891 *Acta Palaeontol. Pol.*, 11, 15–129, 1966.
- 892 Hurcewicz, H.: Siliceous sponges from the Upper Cretaceous of Poland, Part II, Monaxonia
893 and Triaxonia, *Acta Palaeontol. Pol.*, 13, 3–96, 1968.
- 894 Hurd, D.C.: Interactions of biogenic opal, sediment and seawater in the Central Equatorial
895 Pacific, *Geochim. Cosmochim. Ac.*, 37, 10, 2257–2266, 1973.
- 896 Isson, T.T. and Planavsky, N. J.: Reverse weathering as a long-term stabilizer of marine pH
897 and planetary climate, *Nature*, 560(7719), 471–475, 2018.
- 898 Jeans C.V.: Silicifications and associated clay assemblages in the cretaceous marine
899 sediments of southern England, *Clay Miner.*, 13, 101–124, 1978.
- 900 Jurkowska, A.: The biotic-abiotic control of Si burial in marine carbonate systems of the pre-
901 Eocene Si cycle, *Global Biogeochem. Cy.*, 36, e2021GB007079, 2022.
- 902 Jurkowska, A. and Świerczewska-Gładysz, E.: New model of Si balance in the late cretaceous
903 epicontinental European basin, *Global Planet. Change*, 186, 103–108, 2020a.
- 904 Jurkowska, A. and Świerczewska-Gładysz, E.: Evolution of late cretaceous Si cycling
905 reflected in the formation of siliceous nodules (flints and cherts), *Global Planet. Change*, 195,
906 103–334, 2020b.
- 907 Jurkowska, A., Świerczewska-Gładysz, E.: Opoka – a mysterious carbonate-siliceous rock: an
908 overview of general concepts. *Geology, Geophysics & Environment*, 48, 3, 257–278, 2022.
- 909 Jurkowska, A and Świerczewska-Gładysz, E. The evolution of the marine Si cycle in the
910 Archean-Palaeozoic - an overlooked Si source?, *Earth-Science Reviews*, 248, 104-629, 2024.
911
- 912 Jurkowska, A., Świerczewska-Gładysz, E., Bak, M. and Kowalik, S.: The role of biogenic
913 silica in formation of Upper Cretaceous pelagic carbonates and its paleoecological implications,
914 *Cretac. Res.*, 93, 170–187, 2019.
- 915 Jurkowska, A., Uchman, A. and Świerczewska-Gładysz, E.: A record of sequestration of plant
916 material by marine burrowing animals as a new feeding strategy under oligotrophic conditions
917 evidenced by pyrite microtextures, *Palaios*, 33, 312–322, 2018.



- 918 Kastner, M., Keene, J.B. and Gieskes, J.M.: Diagenesis of siliceous oozes. I. Chemical
919 controls on the rate of opal-A to opal-CT transformation-an experimental study, *Geochim.*
920 *Cosmochim. Ac.*, 41, 1041–1059, 1977.
- 921 Kędzierski, M. and Uchman, A.: Bedded chalk marls in the Opole Trough: epicratonic
922 deposits of the Late Cretaceous super-greenhouse episode, in: Haczewski, G. (ed.),
923 *Guidebook for field trips accompanying 31st IAS Meeting of Sedimentology held in Kraków*
924 *on 22nd–25th of June 2015*, Polish Geological Society, Kraków, 145–157, 2001.
- 925 de Kluijver, A., Nierop, K.G.J., Morganti, T.M., Bart, M.C., Slaby, B.M., Hanz, U., de Goeij,
926 J.M., Mienis, F. and Middelburg, J.J.: Bacterial precursors and unsaturated long-chain fatty
927 acids are biomarkers of North-Atlantic deep-sea demosponges, *PLoS ONE*, 16(1), e0241095,
928 <https://doi.org/10.1371/journal.pone.0241095>, 2021.
- 929 Kubiak, A., Pajewska-Szmyt, M., Kotula, M., Leśniewski, B., Voronkina, A., Rahimi, P.,
930 Falahi, S., Heimler, K., Rogoll, A., Vogt, C., Ereskovsky, A., Simon, P., Langer, E., Springer,
931 A., Förste, M., Charitos, A., Joseph, Y., Jesionowski, T. and Ehrlich, H.: Spongin as a Unique
932 3D Template for the Development of Functional Iron-Based Composites Using Biomimetic
933 Approach In Vitro, *Mar. Drugs*. 22, 21(9), 460, <https://doi.org/10.3390/md21090460>, 2023.
- 934 Liguori, B.T.P., de Almeida, M.G. and de Rezende, C E.: Barium and its Importance as an
935 Indicator of (Paleo)Productivity, *Anais da Academia Brasileira de Ciências*, 88, 04, 2093–
936 2103, 2016.
- 937 López-Acosta, M., Potel, C., Gallinari, M., Pérez, F.F. and Leynaert, A.: Nudibranch
938 predation boosts sponge silicon cycling, *Sci. Rep.*, 20, 13(1), 1178.
939 <https://doi.org/10.1038/s41598-023-27411-y>, 2023.
- 940 Mackenzie F.T. and Gees G.: Quartz: Synthesis at Earth-Surface Conditions, *Science*, 173,
941 533–535, 1971.
- 942 Madsen, H.B., Stemmerik, L. and Surlyk, F.: Diagenesis of silica-rich mound-bedded chalk,
943 the Coniacian Arnager Limestone, Denmark, *Sediment. Geol.*, 223, 1–2, 2010.
- 944 Maliva, R.G., Knoll, A.H. and Siever, R.: Secular change in chert distribution: a reflection of
945 evolving biological participation in the silica cycle, *Palaios* 4, 519–532 1989.
- 946 Maliva, R.G. and Siever, R.: Nodular chert formation in carbonate rock, *J. Geol.* 97 (4), 421–
947 433, 1989a.
- 948 Maliva, R.G. and Siever, R.: Chertification histories of some Late Mesozoic and Middle
949 Palaeozoic platform carbonates, *Sedimentology*, 36, 907–926, 1989b.
- 950 Martinez-Ruiz, F., Paytan, A., Gonzalez-Muñoz, M., Jroundi, F., Abad, M., Lam, P., Horner,
951 T. and Kastner, M.: Barite precipitation on suspended organic matter in the mesopelagic zone,
952 *Front. Earth. Sci.*, 8, 567714, <https://doi.org/10.3389/feart.2020.567714>, 2020.
- 953 Meister, P., Herda, G., Petrishcheva, E., Gier, S., Dickens, G.R., Bauer, C. and Liu, B.:
954 Microbial Alkalinity Production and Silicate Alteration in Methane Charged Marine
955 Sediments: Implications for Porewater Chemistry and Diagenetic Carbonate Formation, *Front.*
956 *Earth Sci.*, 9, 756591, <https://doi.org/10.3389/feart.2021.756591>, 2022.



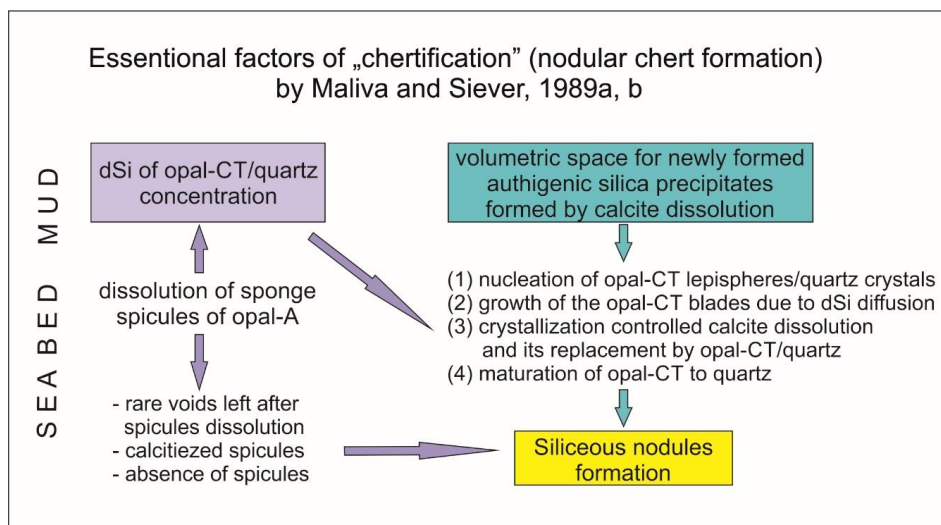
- 957 Murowchick, J.B. and Barnes, H.L.: Effects of temperature and degree of supersaturation on
958 pyrite morphology, *Am. Mineral.*, 72, 1241–1250, 1987.
- 959 Płachno, B., Jurkowska, A., Pacyna G., Worobiec, E., Gedl, P. and Świerczewska-Gładysz,
960 E.: Late Turonian plant assemblage from Opole (southern Poland): new data on Late
961 Cretaceous vegetation of the northern part of European Province in the light of
962 palaeoenvironmental studies, *P. Geologist Assoc.*, 129, 159–170,
963 <https://doi.org/10.1016/j.pgeola.2018.01.008>, 2018.
- 964 Pożaryska, K.: The sedimentological problems of Upper Maastrichtian and danian of Puławy
965 Environment (Middle Vistula), *Biuletyn Państwowego Instytutu Geologicznego*, 81, 1–104,
966 1952.
- 967 Reolid, M.: Pyritized radiolarians and siliceous sponges from oxygen-restricted deposits
968 (Lower Toarcian, Jurassic), *Facies*, 60, 789–799, <https://doi.org/10.1007/s10347-014-0404-6>,
969 [2014](#).
- 970 Reitner, J.: A rare new demosponge from the Solnhofen Lithographic Limestone (Upper
971 Jurassic, Bavaria, Germany), *Doc. naturae*, 192.4, 359–371, 2013.
- 972 Rigby, J. K. and Craig R. C. Demosponges and Hexactinellid Sponges from the Lower Devonian
973 Ross Formation of West-Central Tennessee, *J. Paleontol.* 69, 2, 211–232,
974 <http://www.jstor.org/stable/1306253>, 1995.
- 975 Robert, F. and Chaussidon, M.: A palaeotemperature curve for the Precambrian oceans based
976 on silicon isotopes in cherts, *Nature*, 443, 969–972, 2006.
- 977 Rützler, K. and Macintyre, I.: Siliceous sponge spicules in coral reef sediments, *Mar.*
978 *Biol.*, 49, 147–159, 1978.
- 979 Schieber, J.: Oxidation of detrital pyrite as a cause for marcasite formation in marine lag
980 deposits from the Devonian of the eastern US, *Deep-Sea Res. II*, 54, 1312–1326, 2007.
- 981 Schoonen, M.A.A. and Barnes, H.L.: Reactions forming pyrite and marcasite from solution. I.
982 Nucleation of FeS₂ below 100u C, *Geochim. Cosmochim. Ac.*, 55, 1495–1504, 1991.
- 983 Siever R.: Oceanic silica geochemistry and nodular chert formation, *Geol. Soc. Am., Abstract*
984 *Progress*, 18, 750, 1986.
- 985 Siever, R.: Silica in the oceans: Biological-geochemical interplay, in: Schneider, S. H. and
986 Boston, P.J. (Eds.): *Scientists on Gaia*. MIT Press, Cambridge, 287–295, 1991.
- 987 Siever, R. and Woodford, N.: Sorption of silica by clay minerals, *Geochim. Cosmochim. Ac.*,
988 37, 1851–1880, 1973.
- 989 Stanley, M.S., Ries, J.B. and Hardie, L.A.: Seawater chemistry, coccolithophore population
990 growth, and the origin of Cretaceous chalk, *Geology*, 33, 593–596, 2005.
- 991 Stratmann, T., Simon-Lledó, E., Morganti, T.M., de Kluijver, A., Vedenin, A. and Purser, A.:
992 Habitat types and megabenthos composition from three sponge-dominated high-Arctic
993 seamounts, *Sci Rep.*, 29,12(1),20610, <https://doi.org/10.1038/s41598-022-25240-z>, 2022.



- 994 Sujkowski, Z.: Petrografia kredy Polski. Kreda z głębokiego wiercenia w Lublinie w
995 porównaniu z kredą niektórych innych obszarów Polski, Sprawozdania Państwowego
996 Instytutu Geologicznego, 6, 485–628, 1931.
- 997 Sutton, J., Andre, L., Cardinal, D., Conley, D.J., de Souza, G.F., Dean, J., Dodd, J., Ehlert, C.,
998 Ellwood, M.J., Frings, P.J., Grasse, P., Hendry, K., Leng, M.J., Michalopoulos, P., Panizzo,
999 V.N. and Swann, G.E.A.: A review of the stable isotope bio-geochemistry of the global
1000 silicon cycle and its associated trace elements, *Front. Earth Sci.*, 5, 1–24, 2018.
- 1001 Świerczewska-Gładysz, E.: Late Cretaceous siliceous sponges from the Middle Vistula River
1002 Valley (Central Poland) and their palaeoecological significance, *Ann. Soc. Geol. Pol.*, 76,
1003 227–296, 2006.
- 1004 Świerczewska-Gładysz, E.: Late Turonian and early Coniacian ventriculitid sponges
1005 (Lychniscosida) from Opole Trough (southern Poland) and their palaeoecological
1006 significance, *Ann. Soc. Geol. Pol.*, 82, 201–224, 2012a.
- 1007 Świerczewska-Gładysz, E.: Hexactinellid sponge assemblages across the Campanian-
1008 Maastrichtian boundary in the Middle Vistula River section, central Poland, *Acta
1009 Geol. Pol.*, 62, 561–580, 2012b.
- 1010 Świerczewska-Gładysz, E.: Early Campanian (Late Cretaceous) Pleromidae and
1011 Isoraphiniidae (lithistid Demospongiae) from the Łódź-Miechów Synclinorium (central and
1012 southern Poland): new data and taxonomic revision, *Pap. Palaeontol.*, 2, 189–321, 2016.
- 1013 Świerczewska-Gładysz, E. and Jurkowska, A.: Occurrence and paleoecological significance
1014 of lyssacinoid sponges in the Upper Cretaceous deposits of southern Poland, *Facies*, 59, 763–
1015 777, 2013.
- 1016 Świerczewska-Gładysz, E., Jurkowska, A. and Niedźwiedzki, R.: New data about the
1017 Turonian–Coniacian sponge assemblage from Central Europe, *Cretaceous Res.*, 94, 229–258,
1018 2019.
- 1019 Tatzel, M., von Blanckenburg, F., Oelze, M., Schuessler, J.A. and Bohrmann, G.: The silicon
1020 isotope record of early silica diagenesis, *Earth Planet. Sci. Lett.* 428, 293–303, 2015.
- 1021 Van den Boorn, S.H.J.M., van Bergen, M.J., Nijman, W. and Vroon, P.Z.: Dual role of
1022 seawater and hydrothermal fluids in Early Archean chert formation: evidence from silicon
1023 isotopes, *Geology* 35, 939–942, 2007.
- 1024 Van den Boorn, S.H.J.M., van Bergen, M.J., Vroon, P.Z., de Vries, S.T. and Nijman, W.:
1025 Silicon isotope and trace element constraints on the origin of ~3.5 Ga cherts: implications for
1026 early Archaean marine environments, *Geochim. Cosmochim. Acta* 74, 1077–1103, 2010.
- 1027 Van Dijk, I., de Nooijer, L.J., Hart, M.B. and Reichart, G.-J.: The long-term impact of
1028 magnesium in seawater on foraminiferal mineralogy: mechanism and consequences, *Global
1029 Biogeochem. Cy.*, 30, 438–446, <https://doi.org/10.1002/2015GB005241>, 2016.
- 1030 Vodrážka, R.: A new method for the extraction of microfossils from calcareous rocks using
1031 sulphuric acid, *Palaeontology*, 52, 187–192, 2009.]



- 1032 Von Rad, U. and Rösch, H.: Petrology and diagenesis of deep sea cherts from the Central
1033 Atlantic, in: Hsü, K.J. and Jenkins, H.C. (Eds.), *Pelagic Sediments: On Land and under the*
1034 *Sea*, Sp. Publ. Int. Assoc. Sedimentologists, 1, 327–347, 1974.
- 1035 Walaszczyk, I.: Inoceramid stratigraphy of the Turonian and Coniacian strata in the environs
1036 of Opole (southern Poland), *Acta Geol. Pol.*, 38, 51–61, 1988.
- 1037 Walaszczyk, I.: Integrated stratigraphy of the Campanian–Maastrichtian boundary succession
1038 of the Middle Vistula River (central Poland) section; introduction. *Acta Geol. Pol.*, 62, 4,
1039 485–493, <https://doi.org/10.2478/v10263-012-0027-6>, 2012.
- 1040 Walaszczyk, I., Dubicka, Z., Olszewska-Nejbert, D. and Remin, Z.: Integrated biostratigraphy
1041 of the Santonian through Maastrichtian (Upper Cretaceous) of extra-Carpathian Poland. *Acta*
1042 *Geol. Pol.* 66, 3, 313–350, <https://doi.org/10.1515/agp-2016-0016>, 2016.
- 1043 Williams, L.A. and Crerar, D.A.: Silica diagenesis, II. General mechanisms, *J. Sediment.*
1044 *Petrol.*, 55 (3), 312–321, 1985.
- 1045 Wille, M., Sutton, J., Ellwood, M. J., Sambridge, M., Maher, W., Eggins, S. and Kelly, M.:
1046 Silicon isotopic fractionation in marine sponges: A new model for understanding silicon
1047 isotopic variations in sponges, *Earth Planet. Sc. Lett.* 292, 3–4, 281–289,
1048 <https://doi.org/10.1016/j.epsl.2010.01.036>, 2010.
- 1049 Wise, S.W. and de Weaver, F.M.: Chertification of oceanic sediments, in: Hsü, K.J. and
1050 Jenkyns, H.C. (Eds.), *Pelagic Sediments: On Land and under the Sea*, Sp. Pub. Int. Assoc.
1051 *Sedimentologists*, 1, 301–326, 1974.
- 1052 Xiao, S., Hu, J., Yuan, X., Parsley, R.L. and Ruiji Cao R.: Articulated sponges from the
1053 Lower Cambrian Hetang Formation in southern Anhui, South China: their age and
1054 implications for the early evolution of sponges, *Palaeogeogr. Palaeoclimatol.*, 220, 1–2, 89–117,
1055 2005.
- 1056 Zjilstra, H.J.P.: Early diagenetic silica precipitation, in relation to redox boundaries and
1057 bacterial metabolism in Late Cretaceous Chalk of the Maastrichtian type locality, *Geol.*
1058 *Mijnb.*, 66, 343–355, 1987.
- 1059 Zjilstra, J.J.P.: Sedimentology of the Late Cretaceous and Early Tertiary (Tuffaceous) Chalk
1060 of Northwest Europe, *Geol. Ultraiect.*, 119, 1–192, 1994.
1061
- 1062 **Figure caption:**



1063

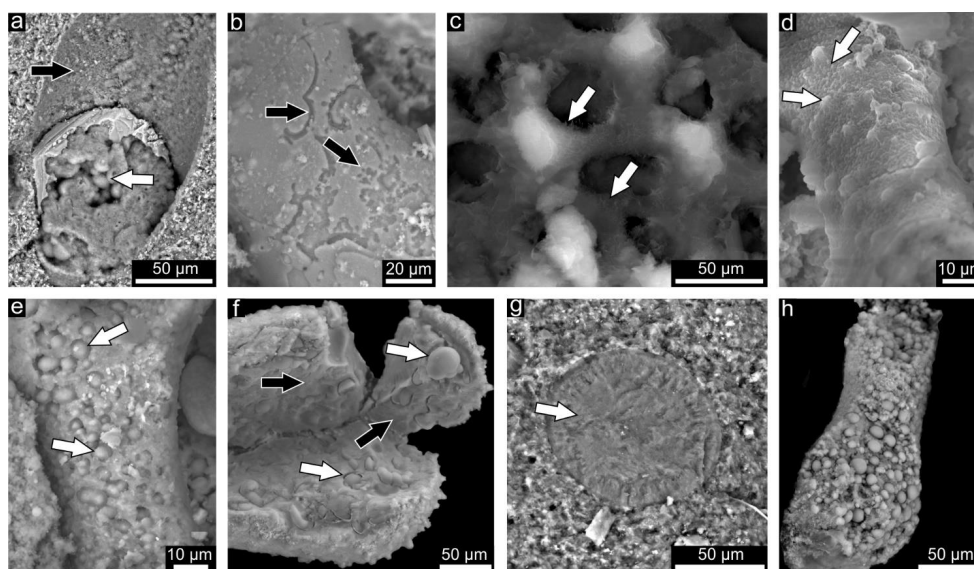
1064

1065

1066

Figure 1. The main assumptions of the classical “chertification” model (Maliva et al., 1989), and essential factors and diagenetic stages of chert formation.

1067



1068

1069

1070

1071

1072

1073

1074

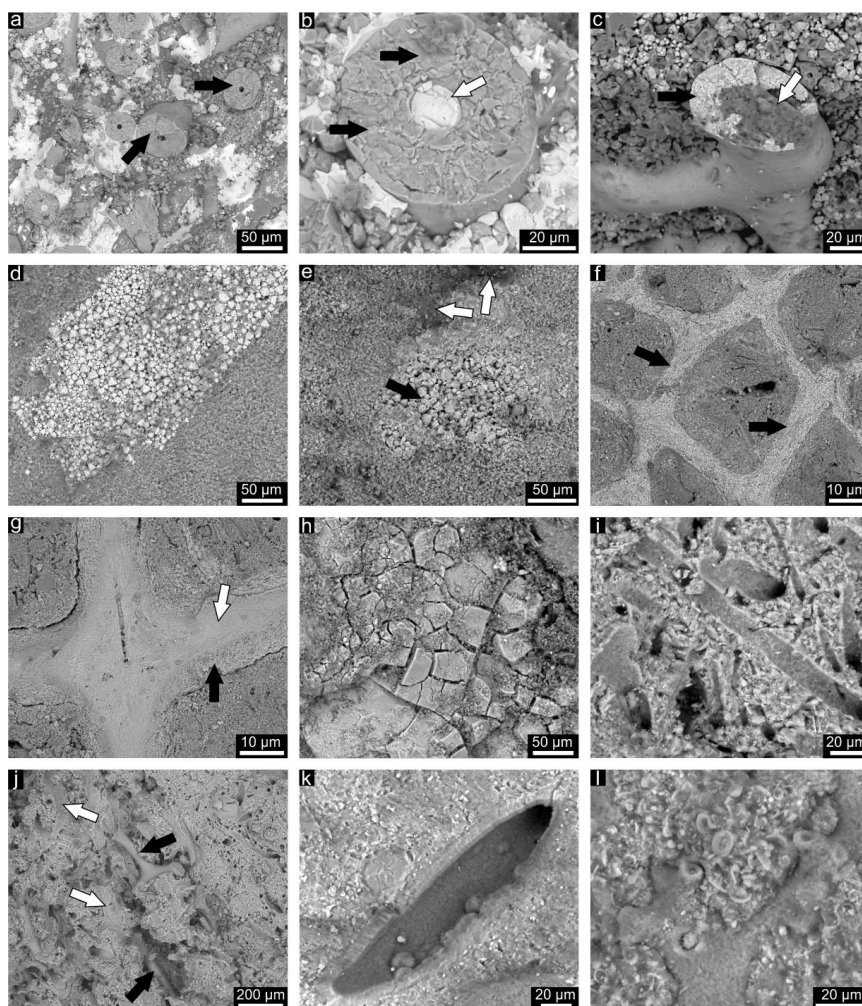
1075

Figure 2. The mineralogy and microtexture of siliceous remnants of sponge loose spicules and rigid skeletons. (a) The siliceous infilling of the spicules with a visible external smooth layer of nano- α -quartz (black arrow) and internal infilling of lepispheres of opal-CT (white arrow); sample Wierzb.1_20 ch. (b) Dissolution remarks formed as cavernous pattern, rounded and platy pits (white arrow) visible on external quartzitic layer of sponge spicule; sample RajN.1_17 op. (c) A dense layer of opal-CT covering (white arrow) the external nano- α -quartz layer of



1076 sponge skeleton; sample Wierzb.1_23 op. (d) Mixed opal-CT clayey/early forms of embryonic
1077 opal-CT layer (white arrow) covering the external surface of sponge spicule; sample
1078 RajN.1_13op. (e) Lepspheres of opal-CT (white arrow) infilling the dissolution rounded
1079 remarks; sample Piotr.1_7 op. (f) The lepispheres of opal-CT (white arrow) cemented by porous
1080 silica (black arrow) infilling the spicule; sample Wierzb.1_16 op. (g) A homogenous dense
1081 mass of nano- α -quartz mixed with opal-CT infilling the sponge spicule (white arrow); sample
1082 Wierzb.1_9 ch-fl. (h) An internal infilling of sponges spicule composed of lepispheres of opal-
1083 CT cemented by porous silica; the external layer of nano- α -quartz is not preserved; sample
1084 Jeż.2_2 ch.

1085



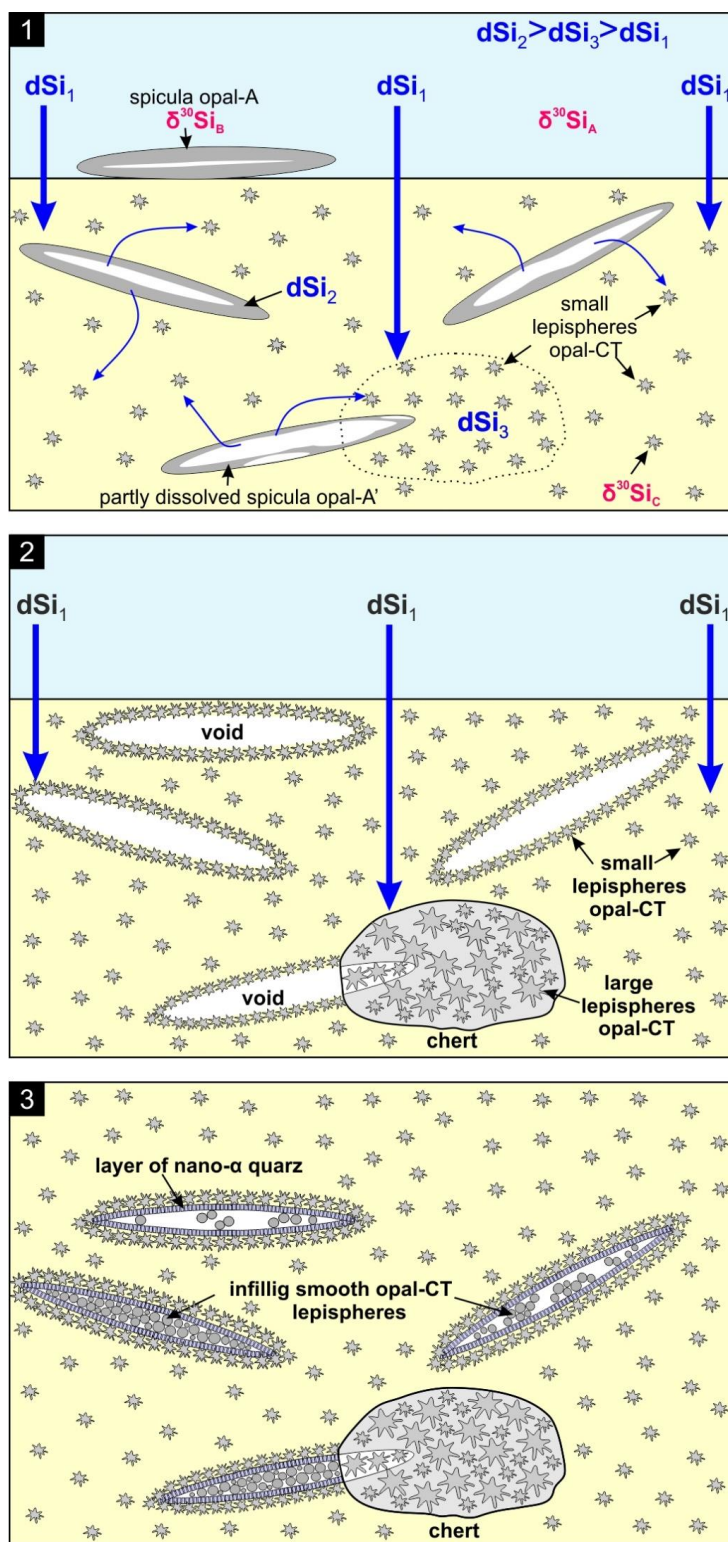
1086

1087

1088 **Figure 3.** The state of preservation of siliceous sponges under the SEM. (a, b) The pyrite and
1089 marcasite infillings of the sponge spicules (black arrow) with visible polycrystalline texture of
1090 pyrite and smooth texture on the external part of the spicule; the white arrow indicates barite;



1091 non-rigid demosponge, upper Turonian marls, sample Fol.7_002. **(c)** The siliceous skeletal
1092 network of lithistid sponge with nano- α -quartz and opal-CT (white arrow) and pyrite with
1093 marcasite infilling; upper Turonian marl, sample Fol.17_001. **(d)** The pyrite crystals outlining
1094 the voids left after the dissolution of hexactinellid sponge spicules; Turonian limestone, sample
1095 Fol.2_001. **(e)** The pyrite crystals with oxidation remarks (black arrow) and associated lumps
1096 of OM (white arrow); hexactinellid sponge, upper Turonian limestone, sample Fol.2_001. **(f)**
1097 The mixed pyrite and ferruginous coatings outlining the previous siliceous skeletal network of
1098 hexactinellid sponge (black arrows); lower Maastrichtian opoka, sample Dziur.14_001. **(g)** The
1099 ferruginous coatings forming a smooth texture inside (white arrow) and with a cavernous
1100 pattern on the outside of the hexactinellid sponge spicule (white arrow); upper Campanian
1101 opoka, sample Piotr.11_001. **(h)** Ferruginous coatings as blocky microtexture; hexactinellid
1102 sponge, middle Campanian opoka, sample Rzeź.19_001. **(i)** The voids left after spicules
1103 dissolution, disperse spicules of non-rigid sponges, Campanian opoka, sample Rzeź.19_001. **(j)**
1104 The voids left after rigid skeleton dissolution of lithistid sponge (white arrow) with some
1105 siliceous infilling of spicules (black arrow) and opoka with voids left after loose spicules
1106 dissolution of non-rigid sponges (top-right); upper Campanian opoka, sample Piotr.12_011. **(k)**
1107 The voids left after spicules dissolution of non-rigid sponges within chert covered by a single
1108 layer of opal-CT; middle Campanian chert, sample Rzeź.9_001. **(l)** The siliceous infilling of
1109 the spicules of lithistid sponge within chert; lower Campanian chert, samples Pniaki.24_002.
1110
1111
1112

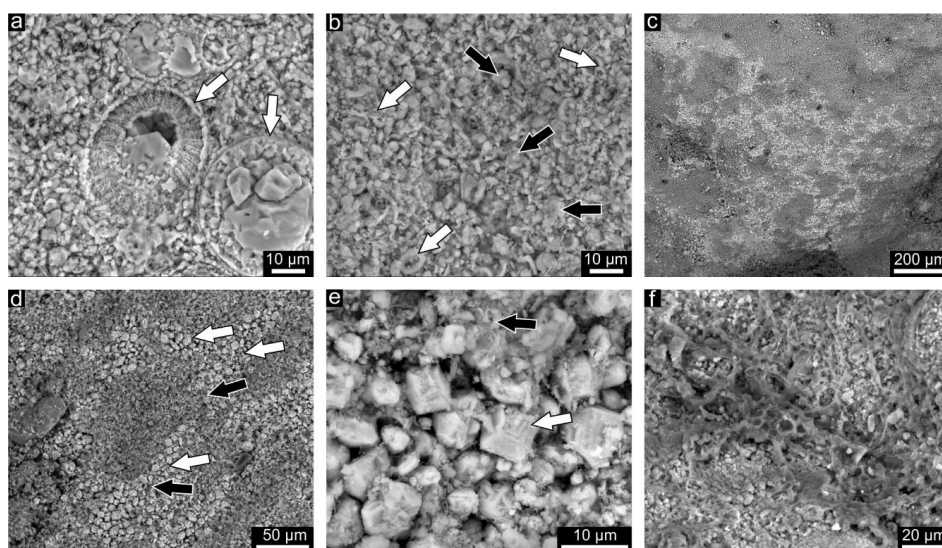




1114

1115

1116 **Figure 4.** The stages of siliceous sponge dissolution followed by secondary silica polymorph
1117 precipitation (opal-CT) under high seawater dSi concentration and the presence of essential
1118 factors for dSi precipitation. Description: text chapter 5.2. The $\delta^{30}\text{Si}_A$ - the Si isotope signature
1119 in a seawater of probably values of hydrothermal (-0.2 to -0.7) (Robert and Chaussidon, 2006)
1120 or seawater (0.7 to 2.2) (Sutton et al., 2018); $\delta^{30}\text{Si}_B$ – the Si isotope signature of sponge spicules
1121 (0 to -6) (Sutton et al., 2018) with more negative values with increasing seawater dSi
1122 concentration (Sutton et al., 2010); $\delta^{30}\text{Si}_C$ -?

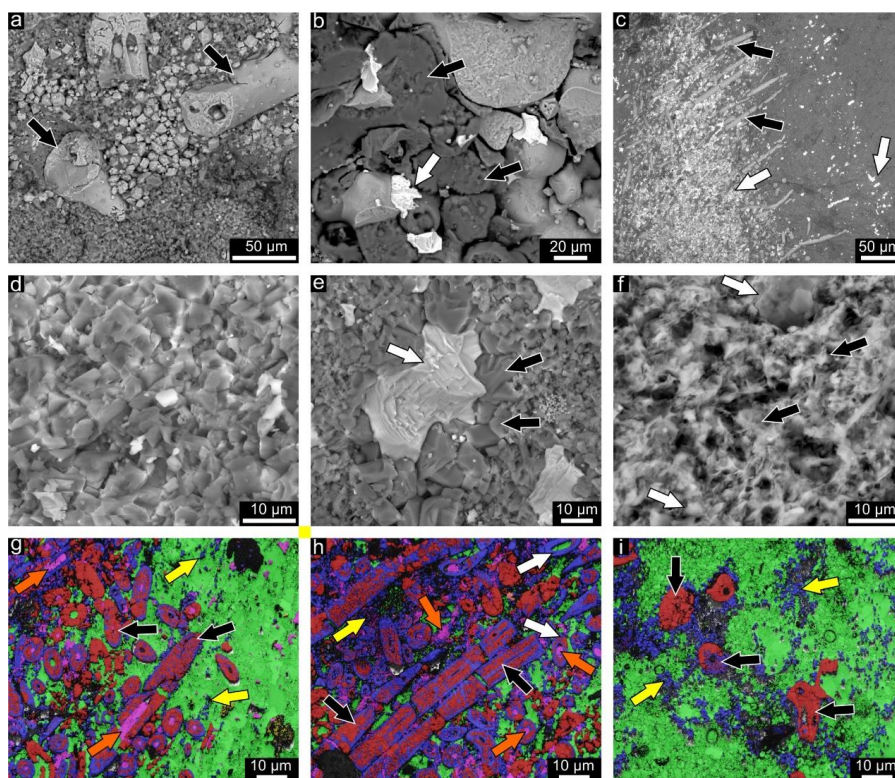


1123

1124

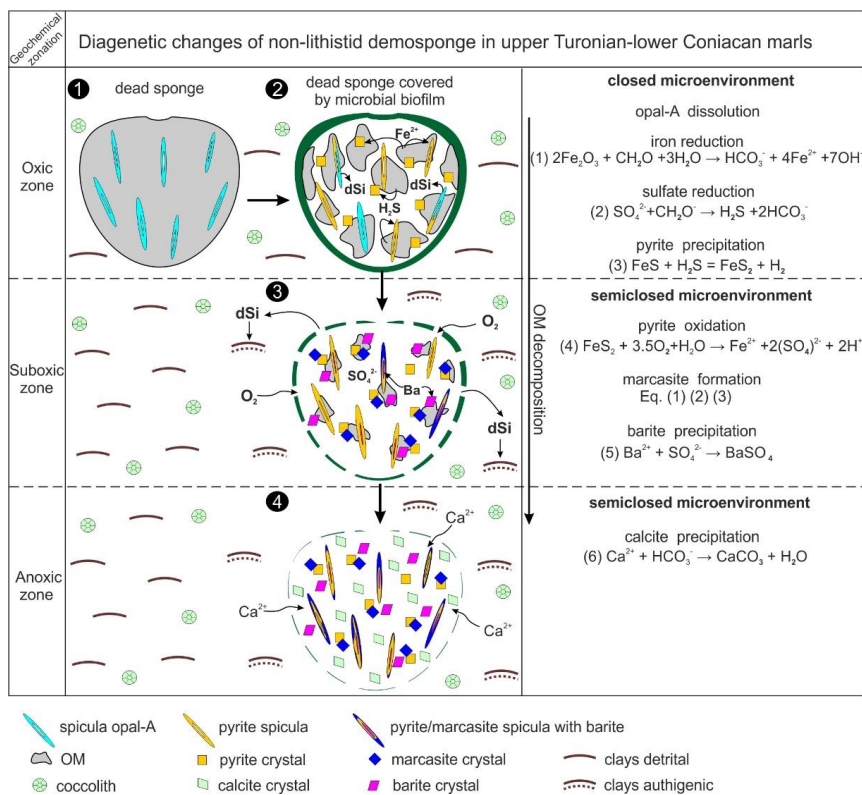
1125 **Figure 5.** Turonian limestone and the state of preservation of siliceous sponges from these
1126 deposits. (a) The common calcispheres of pithonellid assemblages documented in sediment
1127 matrix (white arrow); sample Fol.2_001. (b) The sediment matrix of limestone with visible
1128 allomicritic calcite grains of coccoliths and its fragments (white arrow) and rare authigenic
1129 grains (black arrow); sample Fol.2_002. (c-e) The sponges skeletons are preserved as mixed
1130 euhedral pyrite (white arrow) with subordinate ferruginous (limonite group) coatings (black
1131 arrow) outlining the previous siliceous skeleton; sample: Fol.3_001. (f) The lumps of OM
1132 associated only with sponge skeleton; sample Fol.2_001.

1133



1134

1135 **Figure 6.** The state of preservation of siliceous sponges in upper Turonian–lower Coniacian
 1136 marls. **(a)** The sponge spicules infilled by the polycrystalline pyrite with marcasite (black arrow)
 1137 of hexactinellid sponge; sample Fol.4_001. **(b)** The siliceous skeleton of mixed opal-CT
 1138 and nano- α -quartz (black arrow) with rare barite (white arrow) of lithistid demosponge (type 1
 1139 of preservation); sample Fol.17_001. **(c)** The spicules preserved as massive polycrystalline
 1140 pyrite with marcasite (black arrow) and distribution of barite (white arrow) in non-rigid
 1141 demosponge (type 2 of preservation); sample Fol.7_001. **(d)** The coalescence fused structure
 1142 of authigenic calcite grains infilling the spaces between spicules of non-rigid demosponge;
 1143 sample Fol.7_001. **(e)** The barite (white arrow) surrounded by large sparite crystals (black
 1144 arrow) occurring in deposits infilling the spaces between spicules of non-rigid demosponges;
 1145 sample Fol.7_001. **(f)** The sediment surrounding the hexactinellid sponge fossils with visible
 1146 diagenetically transformed clays (black arrow) and rare authigenic calcite grains (white arrow);
 1147 sample Fol.4_001. **(g-i)** The EBSD analysis (green – calcite, blue – marcasite, red – pyrite,
 1148 purple – barite); the spicules infilled by the pyrite and marcasite (black arrow) and marcasite
 1149 within the sediment (yellow arrow), barite infilling the void left after the dissolution of the
 1150 spicules area around the central canal (orange arrow); non-rigid demosponge, sample Fol.7_001
 1151 (g, h); hexactinellid sponge, sample Fol.4_001 (i).
 1152

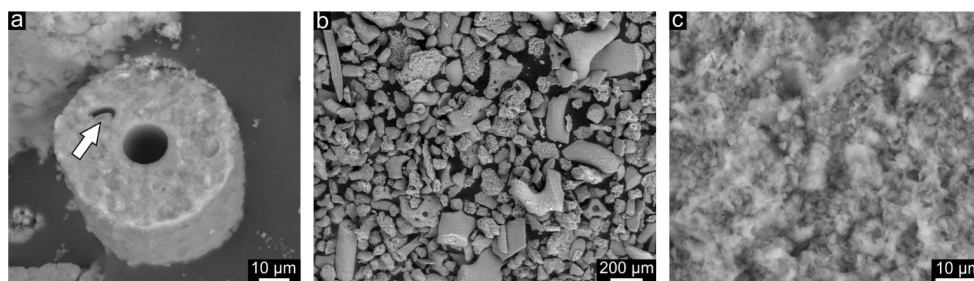


1153

1154

1155 **Figure 7.** The diagenetic changes of non-lithistid demosponges in upper Turonian-lower
1156 Coniacian marls. Description: text chapter 5.3.2.

1157



1158

1159

1160 **Figure 8.** The state of preservation of siliceous sponges in lower-middle Campanian Marls of
1161 MS. (a, b) The siliceous of mixed nano- α -quartz and opal-CT infilling of the sponge spicules
1162 with visible dissolution remarks (white arrow); sample. B.Wlk. 1_4_001. (c) The opal-CT
1163 lepispheres in the sediment matrix of marls; sample Jež.2_5_002.

1164



Section	Age	Lithology	Literature
Opole area: Folwark section	upper Turonian-lower Coniacian	marls, limestone	Alexandrowicz and Radwan, 1973; Walaszczyk, 1992; Kędzierski and Uchman, 2001; Świerczewska-Gładysz, 2012
MS: Jeżówka 2, Wierzbica, Biała Wielka, Pniaki, Rzeżuśnia	lower-middle Campanian	marls	Jurkowska, 2016; Jurkowska and Świerczewska-Gładysz, 2020b; Jurkowska, 2022
MS Jeżówka 2, Wierzbica, Biała Wielka, Rzeżuśnia, Pniaki	lower-middle Campanian	opoka intercalated with cherts	Jurkowska, 2016; Jurkowska and Świerczewska-Gładysz, 2020b; Jurkowska, 2022
MVR: Piotrawin, Raj N, Dziurków, Pawłowice Cm., Dorotka	middle Campanian-lower Maastrichtian	opoka	Walaszczyk, 2012; Walaszczyk et al., 2016; Jurkowska and Świerczewska-Gładysz, 2020a

1165

1166 **Table 1.** Studied sections, lithology and literature.

1167

1168

1169